Scientific Reports

https://doi.org/10.1038/s41598-026-58662-0

Article in Press

Predicting the strength of waste aggregate concrete blocks using novel hybrid machine learning models and graphical user interface deployment

Received: 23 April 2026

Accepted: 16 June 2026

Published online: 25 June 2026

Cite this article as: Arifuzzaman M., Ahmed S.M.S., Khaled M.A. *et al.* Predicting the strength of waste aggregate concrete blocks using novel hybrid machine learning models and graphical user interface deployment . *Sci Rep* (2026). https://doi.org/10.1038/s41598-026-58662-0

Md Arifuzzaman, S. M. Shishir Ahmed, Md. Abdul Khaled, Sameen Yasar Siddiq, Prajnat Barua, Sourov Paul, Md. Mahamudul Hasan, A. K. M. Azad, Muhammad Ali Martuza & Ayed Eid Alluqmani

We are providing an unedited version of this manuscript to give early access to its findings. Before final publication, the manuscript will undergo further editing. Please note there may be errors present which affect the content, and all legal disclaimers apply.

If this paper is publishing under a Transparent Peer Review model then Peer Review reports will publish with the final article.

ARTICLE IN PRESS

© The Author(s) 2026. **Open Access** This article is licensed under a Creative Commons Attribution-NonCommercial-NoDerivatives 4.0 International License, which permits any non-commercial use, sharing, distribution and reproduction in any medium or format, as long as you give appropriate credit to the original author(s) and the source, provide a link to the Creative Commons licence, and indicate if you modified the licensed material. You do not have permission under this licence to share adapted material derived from this article or parts of it. The images or other third party material in this article are included in the article's Creative Commons licence, unless indicated otherwise in a credit line to the material. If material is not included in the article's Creative Commons licence and your intended use is not permitted by statutory regulation or exceeds the permitted use, you will need to obtain permission directly from the copyright holder. To view a copy of this licence, visit http://creativecommons.org/licenses/by-nc-nd/4.0/.

ARTICLE IN PRESS

Waste-Aggregate Concrete Blocks: Novel Hybrid Machine Learning-Based Models for Strength Prediction- ICE, and GUI Deployment

Md Arifuzzaman[a*], S.M. Shishir Ahmed[b], Md. Abdul Khaled[c], Sameen Yasar Siddiq[b], Prajnat Barua[d], Sourov Paul[e], Md. Mahamudul Hasan[b], A. K. M. Azad[f], Muhammad Ali Martuza[g] and Ayed Eid Alluqmani[h*]

[a] King Faisal University, Department of Civil and Environmental Engineering, College of Engineering, P.O. Box 380, Al-Ahsa 31982, Saudi Arabia

[b] Department of Civil Engineering, Military Institute of Science and Technology (MIST), Dhaka, Bangladesh

[c] Department of Civil Engineering, Ahsanullah University of Science and Technology (AUST), Dhaka, Bangladesh

[d] Department of Civil and Environmental Engineering, North South University (NSU), Dhaka, Bangladesh

[e] Department of Civil Engineering, Leading University, Sylhet-3112, Bangladesh

[f] Department of Mathematics and Statistics, Faculty of Science, Imam Mohammad Ibn Saud Islamic University (IMSIU), 13318, Riyadh, Kingdom of Saudi Arabia

[g]Department of Computer Engineering, College of Computer, Qassim University, Buraydah, 51452, Saudi Arabia

[h] Department of Civil Engineering, Faculty of Engineering, Islamic University of Madinah, Prince Naif Ibn Abdulaziz, 42351, Medina, Kingdom of Saudi Arabia

*Corresponding Author: E-mail: marifuzzaman@kfu.edu.sa (Md Arifuzzaman)

E-mail: sourovpaul6782@gmail.com (Sourov Paul)

ARTICLE IN PRESS

Abstract:

Concrete blocks made from waste aggregates have become a promising way to reduce waste and conserve natural resources while still offering good mechanical performance in both solid and hollow concrete blocks. This is especially relevant as more sustainable construction projects increasingly use recycled and alternative materials. This research develops a series of novel hybrid machine learning (ML) models to accurately predict compressive strength, using a dataset of 544 concrete samples from various sources. The six novel hybrid ML frameworks are designed as Hybrid Stacked Ensemble (HSE), Hybrid Residual Learning (HRL), Hybrid Weighted Ensemble (HWE), Hybrid Meta-Learning (HML), Hybrid Bayesian Stacking (HBS), and Hybrid Feature Fusion (HFF). Results show that novel Hybrid Bayesian Stacking (HBS) algorithms deliver excellent predictive accuracy across all evaluation metrics, with (R^2 = 0.998, RMSE = 0.665) during training and (R2 = 0.987, RMSE = 1.836) during testing. Furthermore, Individual Conditional Expectation (ICE) and SHapley Additive exPlanations (SHAP) analyses identified important input features and their effects on compressive strength. A graphical user interface (GUI) was developed to make predictive models accessible for practical engineering use. This

ARTICLE IN PRESS

research presents a novel hybrid ensemble technique that is reliable and effective for modelling concrete behaviour, enabling engineers to make accurate predictions.

Keywords: Concrete block; Waste aggregate; Hybrid Bayesian stacking ensemble; SHAP interpretability; Individual Conditional Expectation; Compressive strength prediction; Sustainable construction; GUI deployment.

Abbreviation	Full Term
HCB	Hollow Concrete Block
RA	Recycled Aggregate
FA	Fine Aggregate
CA	Coarse Aggregate
W/C	Water-to-Cement ratio
ML	Machine Learning
ANN	Artificial Neural Network
MLP	Multi-Layer Perceptron
RF	Random Forest
XGB	Extreme Gradient Boosting
LGBM	Light Gradient Boosting Machine
CB	CatBoost
GB	Gradient Boosting
PCA	Principal Component Analysis
SHAP	SHapley Additive exPlanations
ICE	Individual Conditional Expectation
GUI	Graphical User Interface
HSE	Hybrid Stacked Ensemble
HRL	Hybrid Residual Learning
HWE	Hybrid Weighted Ensemble
HML	Hybrid Meta-Learning
HBS	Hybrid Bayesian Stacking
HFF	Hybrid Feature Fusion
R^2	Coefficient of Determination
RMSE	Root Mean Squared Error
SI	Scatter Index
PI	Performance Index
U95	95 % Uncertainty Band
T-stat	t-Statistic of Residuals
OBJ	Composite Objective Function
SCI	Scatter Compactness Index
EVS	Explained Variance Score

ARTICLE IN PRESS

ARTICLE IN PRESS

1. Introduction

Concrete is one of the most extensively utilized construction materials worldwide, with global production exceeding 30 billion tons annually [1]. Ordinary Portland Cement (OPC), the main ingredient in concrete, is harmful to the environment due to its production. About 5 to 8 percent of the world's CO_2 emissions come from making cement. By 2060, production could reach 4 to 6 billion tons per year, which would make climate change even worse [2–4]. This damage to the environment has made people call for long-lasting options to making concrete, like using waste materials and extra cementitious materials (SCMs) instead of cement and aggregates in some cases [5]

Recycled concrete aggregates (RCA) derived from construction and demolition waste have been widely studied for use in concrete. Recent studies have shown that the proper treatment and handling of RCA can reduce its water absorption to about 3.0%. This means that it can be used to replace up to 50% of natural aggregates without losing much strength [6,7]. But because mortar is stuck to RCA particles, they tend to be more porous and absorb more water than natural aggregates. This means that the mix design needs to be carefully optimized [8]. Rice husk ash (RHA) is made by burning agricultural waste under controlled conditions at temperatures between 550 and 700 °C. It has very pozzolanic properties and has shown promise in making concrete last longer and be stronger when used as a partial cement replacement at amounts of 10 to 30 % [9–11]. In the same way, fly ash (FA) from thermal power plants has pozzolanic action that helps build strength over time and makes things last longer [12]. Studies have demonstrated optimal RHA replacement levels of 10-20% to maximize compressive strength, with higher replacement rates leading to reduced strength due to insufficient calcium hydroxide availability [13].

Hollow concrete blocks (HCBs), which constitute a significant portion of masonry construction materials, offer substantial potential for incorporating waste materials. Some industry wastes, like fly ash, blast furnace slag, silica fume, and steel scrap, and some agricultural wastes, like rice husk ash, bagasse ash, and coconut shells, have been looked at as possible alternatives to cement and aggregates in the production of concrete [14–18]. The utilization of these waste materials not only addresses disposal challenges but also contributes to energy conservation, natural resource preservation, and reduced raw material costs [19]. Fly ash, characterized by spherical particles and pozzolanic properties, improves workability and long-term strength development when used at replacement levels of 20-30% [20]. Additionally, EMV-fabricated RAC improved compressive strength and elasticity, delayed damage progression, and showed distinct compressive and tensile size-effect behaviours [21]. Ground granulated blast furnace slag has latent hydraulic qualities and has been shown to make concrete last longer and be less likely to break down when exposed to sulfate [22]. Studies on hollow concrete blocks with 100% RCA replacement have demonstrated structural soundness and compliance with international standards when properly designed [23].

ARTICLE IN PRESS

Despite the demonstrated viability of incorporating waste materials into concrete, accurately predicting compressive strength remains a critical challenge [24,25]. Traditional empirical models, based primarily on the water-cement ratio and curing age, fail to adequately capture the complex interactions among multiple mixture components, particularly when dealing with heterogeneous waste materials [26]. The traditional way of checking strength involves curing for 28 days, then performing destructive tests. This takes a lot of time, work, and money. Because of these problems, it is hard for leftover materials to be widely used in concrete production. This is because engineers need accurate predictive tools to assess concrete quality and develop the best mix design [27,28]

In recent years, machine learning (ML) methods have become strong alternatives to old empirical models for guessing the mechanical properties of concrete [29–32]. Studies have shown that different machine learning models used to predict the strength of concrete have coefficient of determination (R^2) values higher than 0.95 [33,34]. However, individual ML models possess inherent limitations: ANNs are susceptible to overfitting and require extensive hyperparameter tuning, decision tree-based models exhibit instability with data variations, and linear models cannot adequately represent complex nonlinear interactions [35,36]. To overcome the limitations of single models, ensemble learning approaches have gained prominence in recent literature [37]. Stacking ensemble learning, which uses a meta-learner to combine predictions from multiple base models in the best possible way, has shown strong promise for real-world applications. Using random forest, gradient boosting decision trees, XGBoost, and LightGBM as base learners and linear regression as the meta-learner [38]. Li and Song [39] showed that the stacking ensemble model did a much better job of predicting the strength of rice husk ash concrete than individual methods. Similarly, research on ultra-high-performance concrete has shown that stacking regressors combining XGBoost, CatBoost, LightGBM, and Extra Trees can achieve R^2 values exceeding 0.98 [40,41].

Building on ensemble learning foundations, hybrid machine learning approaches integrate multiple methodologies, including different algorithm families, feature engineering techniques, and optimization strategies, to create sophisticated predictive frameworks. Bayesian optimization combined with stacked ensemble learning has been shown to enhance model performance through systematic hyperparameter tuning significantly [42,43]. Meta-learning approaches, which learn from predictions of multiple diverse models, have demonstrated exceptional performance with R^2 values exceeding 0.93 for structural engineering applications [44]. Residual learning frameworks, where a secondary model learns to predict the errors of a base model, offer advantages in scenarios with systematic prediction biases [45]. Feature fusion strategies that combine predictions from models trained on different feature representations have shown improved performance through multi-view learning [46]. Despite these advances, comprehensive investigations comparing multiple hybrid architectures specifically for hollow concrete blocks with waste aggregates remain limited in the literature.

1.1 Literature Review

ARTICLE IN PRESS

Over the past ten years, the use of machine learning methods to predict the compressive strength of concrete has grown by a significant amount. This is because computers have become faster, and more experimental data is available. In the beginning, artificial neural networks (ANNs) were mostly used because they could describe complicated, nonlinear relationships between input parameters and outputs [47,48]. Subsequent research by Ni et al. [49] established that multilayer perceptron (MLP) architectures with properly configured hidden layers could achieve mean absolute percentage errors below 10% for diverse concrete mixtures.

Recently, tree-based ensemble methods have become more popular because they are reliable, easy to understand, and perform well across a wide range of real-world situations. Extreme Gradient Boosting (XGBoost), which was created by Chen and Guestrin [50], has proven to be very good at predicting the strength of concrete. Feng et al. [51] showed that XGBoost could get R^2 values higher than 0.96 for high-performance concrete while giving feature importance scores that were in line with principles of concrete science. Light Gradient Boosting Machine (LightGBM) and Categorical Boosting (CatBoost) represent recent innovations that offer improved computational efficiency and native handling of categorical variables [52,53]. Comparative studies have shown that these gradient boosting variants consistently outperform traditional algorithms such as linear regression, decision trees, and support vector machines for concrete applications [54,55].

Research by Zhang et al. [56] established that RF models could effectively capture the complex interactions among mixture components, aggregates, and curing conditions, achieving prediction accuracies comparable to neural networks while significantly reducing training time. Support vector regression (SVR), while less commonly employed than tree-based methods, has shown competitive performance for datasets with moderate sample sizes, particularly when combined with appropriate kernel functions and hyperparameter optimization [57,58]. Li and Song [39]created a stacking ensemble model for rice husk ash concrete that uses RF, GBDT, XGBoost, and LightGBM as base learners and linear regression as the meta-learner. This model performs much better than individual models. Similar success has been reported for ultra-high-performance concrete, where stacking ensembles combining XGBoost, CatBoost, LightGBM, and Extra Trees achieved R^2 values exceeding 0.98 [59].

Bayesian optimization has become an effective method for systematic hyperparameter tuning in ensemble models [60]. Conventional hyperparameter optimization techniques, such as grid search and random search, become computationally impractical for ensemble models with numerous hyperparameters. Bayesian and PSO optimisation tackle this issue by developing a probabilistic surrogate model of the objective function and employing acquisition functions to direct the search towards favourable hyperparameter configurations [61,62]. Recent research has demonstrated that Bayesian-optimised stacking ensembles can achieve superior performance compared to manually tuned or grid-searched alternatives while requiring significantly fewer function evaluations [63,64]. Meta-learning approaches extend the ensemble learning concept by training models to learn from the learning process itself [65]. In the context of concrete strength prediction, meta-learning involves combining multiple base models trained on different feature representations or

ARTICLE IN PRESS

data subsets, with a meta-model learning to weight their contributions based on input characteristics optimally [66]. Research on steel fiber-reinforced concrete has shown that meta-learning architectures can achieve mean absolute errors below 0.4 MPa while providing enhanced generalization to unseen mixture designs [67].

Residual learning frameworks, inspired by deep learning architectures such as ResNet, have been adapted for concrete strength prediction with promising results [68,69]. The core concept involves training a primary model to make initial predictions, followed by a secondary model that learns to predict the residuals (prediction errors) of the primary model [70]. The final prediction combines both models, effectively enabling progressive refinement of estimates. Feature fusion strategies represent another innovative hybrid approach that combines predictions from models trained on different feature representations [71]. The diverse perspectives captured by different feature representations can be combined through weighted averaging or meta-learning to produce more robust predictions [72,73]. Recent applications of SHAP to concrete strength prediction have demonstrated that ML models learn relationships consistent with established principles of concrete science [74]. Similarly, research on recycled aggregate concrete has used SHAP to confirm that the percentage of aggregate replacement exhibits nonlinear effects, with optimal ranges varying by waste material type [75,76].

1.2 Research Gaps

This research systematically addresses these gaps by (1) focusing specifically on hollow concrete blocks with comprehensive waste material incorporation; (2) developing and comparing six distinct novel hybrid ML architectures with complementary strengths; (3) utilizing a comprehensive dataset spanning multiple waste types including recycled aggregates, industrial by-products, and agricultural wastes; (4) integrating Individual Conditional Expectation (ICE) and SHAP interpretability analysis throughout the modeling process; (5) employing rigorous validation protocols including k-fold cross-validation and comprehensive performance metrics; and (6) developing a practical GUI application for industrial deployment. The combination of advanced hybrid modeling, domain-specific focus, comprehensive interpretability analysis, and practical deployment tools positions this research to make significant contributions toward sustainable, data-driven concrete technology.

1.3 Research significance

The present research is crucial because it establishes a rigorous, data-driven system for accurately predicting the compressive strength of sustainable hollow and solid concrete blocks made from waste aggregates. This directly supports both the goals of structural safety and environmental protection. The tool uses standard mixture parameters, such as coarse aggregate (CA), fine aggregate (FA), water–cement ratio (W/C), binder content, and curing age, as input features. Additionally, the main methodological contribution is the development of six advanced novel hybrid machine learning frameworks that combine different base learners and meta-learners. These

ARTICLE IN PRESS

novel hybrid models perform very well, especially the Hybrid Bayesian Stacking (HBS) method, which achieves a coefficient of determination close to 1. This shows that advanced ensemble strategies can yield near-experimental accuracy when estimating compressive strength.
Beyond predictive accuracy, incorporating SHAP and ICE analyses provides crucial interpretability, enabling engineers to identify the most influential parameters, such as coarse aggregate (CA), fine aggregate (FA), and curing age, thereby facilitating knowledge-driven engineering decisions. Additionally, a graphical user interface (GUI) makes these models practically deployable, bridging the gap between advanced computational intelligence and day-to-day structural engineering practice. Furthermore, this research not only provides immediate practical benefits but also lays a strong foundation for future work on code development, reliability assessment, and the use of hybrid ML techniques for other performance indicators, such as the durability, shrinkage, or thermal properties of environmentally friendly concrete blocks.

2. Materials and Methods

2.1. Database

The database used in this study was compiled from experimental results reported in 19 independent, peer-reviewed journal articles on hollow and solid concrete blocks containing waste materials as partial replacements for cement, fine aggregate, or coarse aggregate, published between 2009 and 2025, as listed in **Appendix 1.** In this study, a total of 544 data points were collected from experiments and existing studies to predict the compressive strength of HCB that uses waste materials as aggregates and binders. In these experiments, different mix designs have been created using various recyclable materials. Binder, fine aggregate, and coarse aggregate were replaced with 21 types of recyclable materials to conduct the experiments. The highest 93 of these data used rice husk ash as the replacement material. Banana leaf ash was used in 60% of the data, ranking as the second-most-substituted material. The main objective of this study is to identify the variables that have most strongly influenced the mechanical performance of these blocks.

ARTICLE IN PRESS

2.1.1. Selection criteria

To ensure the consistency and reliability of the compiled database, strict inclusion and exclusion criteria were applied during data collection. Only studies reporting complete mixture proportions and experimentally measured compressive strength values were included. The selected studies were required to have essential input variables, including recycled aggregate content, water-to-cement ratio, binder content, fine aggregate content, coarse aggregate content, and curing age. Studies with incomplete mix design information, missing compressive strength values, duplicate datasets, inconsistent units, or unclear testing procedures are excluded from the database.

All data collected from different studies have been standardized to consistent engineering units prior to model development. The compressive strength values are converted into MPa, while material quantities are converted into kg/m^3. Duplicate records have been carefully checked and removed to avoid bias during model training. Data consistency and numerical ranges were also verified via statistical screening prior to preprocessing.

ARTICLE IN PRESS

2.1.2. Compression Testing Standards and Block Specifications

The concrete blocks used in the database have been experimentally tested in the original studies using standard compressive strength testing procedures. Most of the selected experiments followed ASTM C140, ASTM C39, BS EN 772, or equivalent international standards for determining compressive strength. The database includes both hollow and solid concrete blocks with varying dimensions and geometries depending on the original experimental programs. In most studies, load application during compression testing was performed under monotonic axial loading conditions using calibrated compression testing machines.

Although minor variations existed among experimental studies in specimen dimensions and curing environments, only studies that followed acceptable standard testing methodologies have been incorporated into the database to maintain data consistency and reliability.

2.2. Concrete block

A robust mix of cement, sand, and coarse aggregates is used to make concrete blocks. The ratio of cement to sand to aggregate is usually 1:3:6 or 1:2:4, depending on the required block strength. The mix is designed to have a low water-to-cement ratio to ensure greater stability and longer-term durability.

Blocks are rectangular pieces of material with controlled dimensions. Its density can range from light to heavy depending on the construction purpose. Concrete blocks are more effective at retaining heat and sound than regular clay bricks, particularly because they are light or hollow. Additionally, they resist fire more effectively. Concrete blocks are significant because they speed up the construction process, reduce mortar joints, and produce masonry of the same quality. They are commonly used for walls that bear forces and those that don't, as well as for partitions, boundary walls, and other masonry elements in housing and infrastructure projects.

ARTICLE IN PRESS

2.2.1 Hollow concrete block

Hollow blocks use similar concrete mixes, but they are often made with lower-density aggregates or partial replacements to make them lighter and better at retaining heat. They are most often used as non-load-bearing structures, so their compressive strength is typically lower.

They have large voids inside, usually occupying more than 25% of the volume, which makes them lighter and better at insulating against sound and heat, but they are a little less durable than solid blocks. Bulk density can be either normal-weight or lightweight, making it easier to handle and reducing the dead load on structures. Hollow blocks are essential for quickly and cheaply building non-load-bearing and medium-load-bearing walls, infill walls in frames, and partitions. When additional structural capacity is needed, such as in reinforced masonry walls, columns, or shear walls, their cavities can be filled with grout or reinforced.

ARTICLE IN PRESS

2.2.2 Solid concrete block

Solid blocks have a denser, often richer concrete mix that gives them higher compressive strengths. It's usually left out with big holes, so the entire section adds to strength and mass per unit. Physically, solid, dense blocks are often used in pavements or structures that need to withstand high pressure. Their compressive strengths are usually higher than those of hollow concrete blocks. Because they are denser, they don't insulate heat as well as lightweight or hollow blocks. Solid blocks are crucial in places where large loads must be supported and strength is required, such as foundations, retaining walls, basement walls, and heavily loaded bearing walls. They are also used for paving, columns, and other structural masonry applications where strength and impact resistance are more important than weight loss.



Figure 1(a): Commercial solid and hollow concrete blocks



Figure 1(b): Use of concrete block in a residential building construction

ARTICLE IN PRESS

2.3. Statistical overview of the data

Figure 2 presents the distribution of all input features within the compiled database. Curing age is predominantly concentrated between 14 and 56 days, reflecting standard testing conditions. Recycled aggregate content is heavily skewed toward lower dosages, with most specimens below 50 kg/m³, indicating limited replacement levels in the surveyed studies. Coarse aggregate similarly clusters below 600 kg/m³, while fine aggregate shows a distinctive concentration exceeding 1000 kg/m³. Binder content is relatively balanced across the 200–400 kg/m³ range, suggesting diverse mix proportions. The water-to-cement ratio is reasonably well spread between 0.4 and 0.6, covering a practical design spectrum. Compressive strength, however, is strongly concentrated in the 0–5 MPa range, which is characteristic of hollow masonry units, with progressively fewer specimens representing higher strength categories.

To facilitate unbiased model development and generalisation assessment, the compiled dataset was partitioned into mutually exclusive training (80%; n = 432) and testing (20%; n = 108) subsets via random, stratified allocation, with the statistical characteristics of both phases reported in **Table 1**. The close agreement between training and testing descriptors, evidenced by near-identical mean

ARTICLE IN PRESS

W/C ratios (0.51 vs. 0.51), binder contents (240.39 vs. 243.83 kg/m³), and FA concentrations (1132.97 vs. 1134.54 kg/m³), confirms that the partitioning preserved the underlying distributional structure of the parent population, thereby minimising the risk of data leakage or phase-specific bias. Compressive strength exhibited pronounced right-skewed heterogeneity across both phases, spanning 0.41–93.28 MPa in training and 0.31–67.6 MPa in testing, with standard deviations of 17.55 and 16.57 MPa, respectively, reflecting the inherently wide mechanical variability associated with diverse HCB mix formulations incorporating recycled constituents.

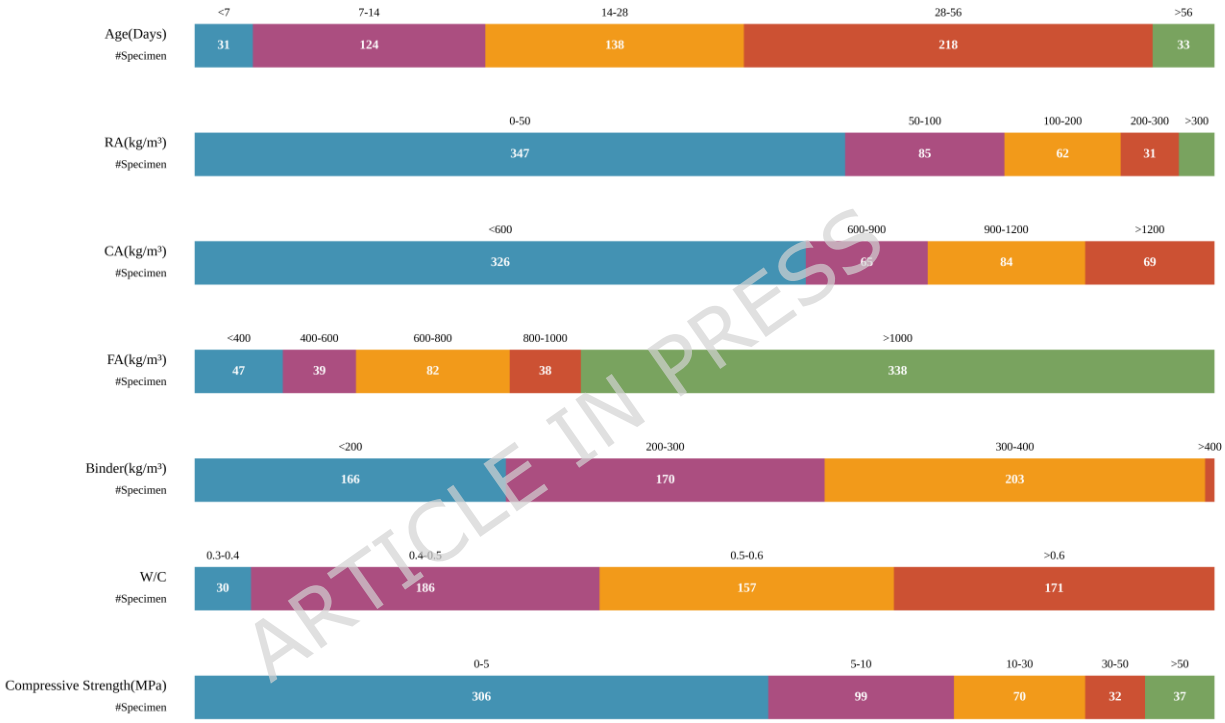


Fig. 2. Distribution of input features of the concrete blocks database.

Table 1: Statistical distribution of database features.

Statistical Parameters	Phase	RA (kg/m^3)	W/C	Binder (kg/m^3)	FA (kg/m^3)	CA (kg/m^3)	Age (Days)	Compressive Strength (MPa)
25th Percentile	Training	10.4	0.45	152.03	686.24	0	7	2.13
	Testing	9.82	0.45	170.27	696	0	7	2.5
50th Percentile	Training	29.76	0.5	255	1131.43	0	21	4.3
	Testing	30	0.5	261	1131.43	0	28	3.94
75th Percentile	Training	80	0.6	326	1620.75	960.2	28	11.5
	Testing	73.93	0.6	326	1610.6	1126	28	7.9
Maximum	Training	414	0.63	438	2084.5	1470	91	93.28
	Testing	349	0.63	415.8	2084.5	1470	91	67.6

ARTICLE IN PRESS

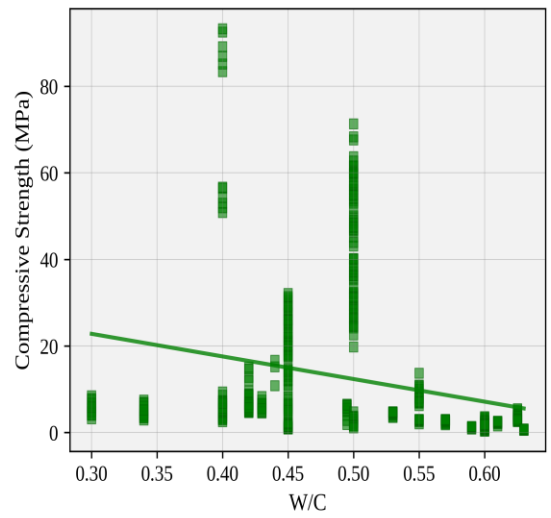
Mean	Training	66.64	0.51	240.39	1132.97	439.64	21.51	12.04
	Testing	58.66	0.51	243.83	1134.54	433.78	22.5	11.14
Minimum	Training	0	0.3	58.6	210.13	0	1	0.41
	Testing	0	0.3	58.6	210.13	0	1	0.31
SD	Training	90.29	0.09	97.9	519.51	551.31	15.35	17.55
	Testing	70.12	0.08	97.1	523.28	570.19	15.88	16.57

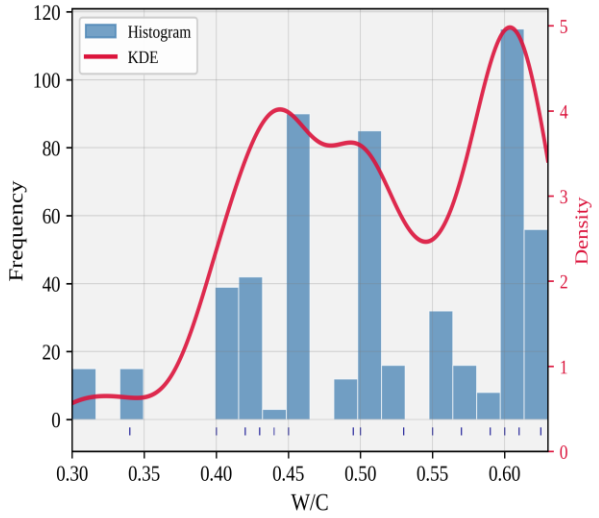
2.4. Parametric study

The bivariate relationships between compressive strength and each input parameter are examined through scatter plots with linear best-fit trajectories, supplemented by corresponding frequency histograms and kernel density estimation (KDE) curves, as presented in **Fig.3**. CA content exhibited the most pronounced positive association with compressive strength, with the scatter plot revealing a clear ascending trend across the CA range of 0–1470 kg/m³, corroborating the well-established role of skeletal aggregate in enhancing the load-bearing matrix of masonry blocks. Binder content similarly showed a discernible positive trend, with compressive strength values progressively exceeding 200 kg/m³. The corresponding bimodal KDE, exhibiting dual density peaks near 90 and 325 kg/m³, reflects the heterogeneous binder proportioning strategies documented in the consolidated literature. Curing age manifested a positive monotonic trend consistent with continued hydration-driven strength gain, with the histogram revealing a pronounced concentration of specimens at the standard testing ages of 7, 14, and 28 days, confirming the conventional curing protocols adopted by contributing studies. Conversely, the W/C ratio displayed a negative linear trajectory with high-strength specimens (>50 MPa) clustered at W/C values between 0.40 and 0.45, and a bimodal frequency distribution peaking near 0.45 and 0.60, indicative of two distinct mix design philosophies within the database. FA content showed a modest inverse trend with compressive strength, with most high-FA specimens registering strengths below 10 MPa, whereas recycled aggregate exhibited a comparatively weak and diffuse negative association, attributable to the interfacial transition zone weakening commonly associated with elevated substitution levels.

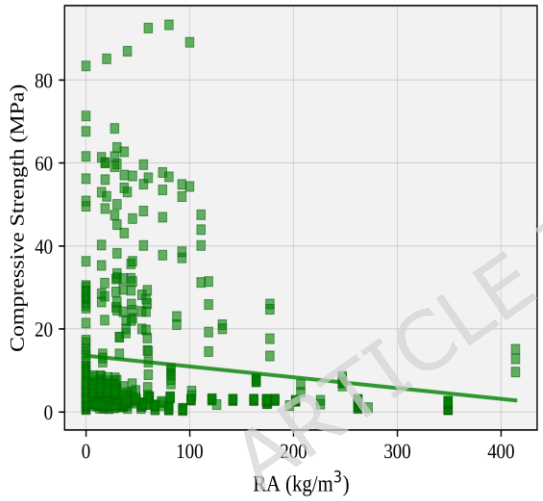
ARTICLE IN PRESS

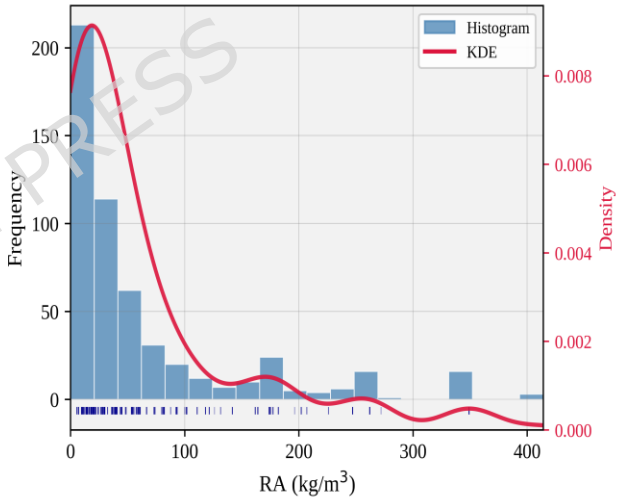
(a)



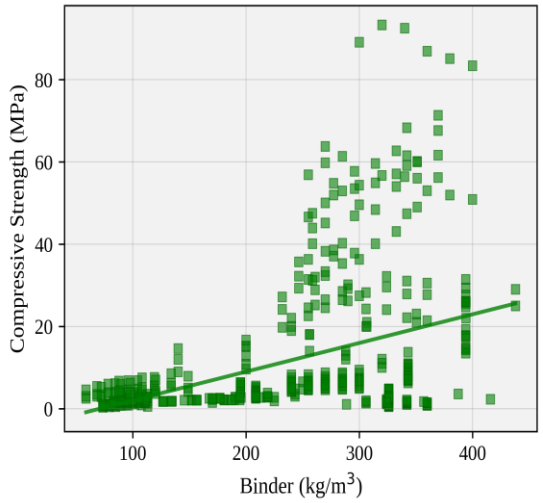


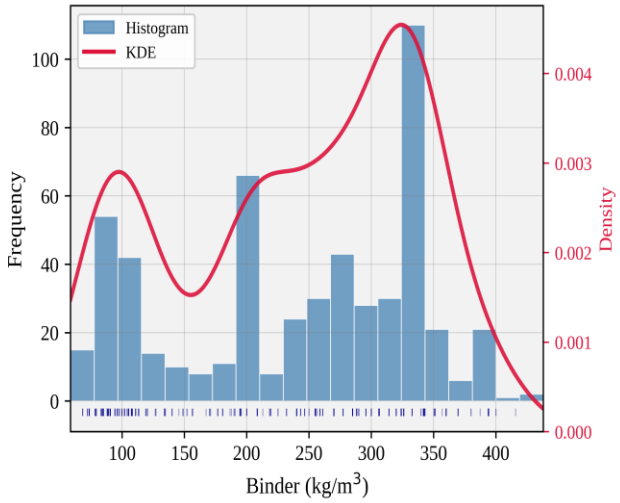
(b)





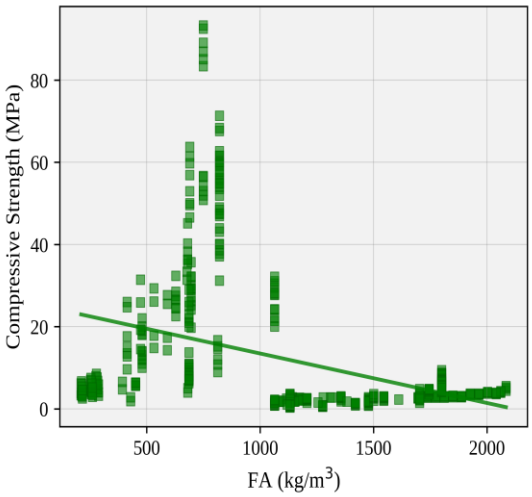
(c)

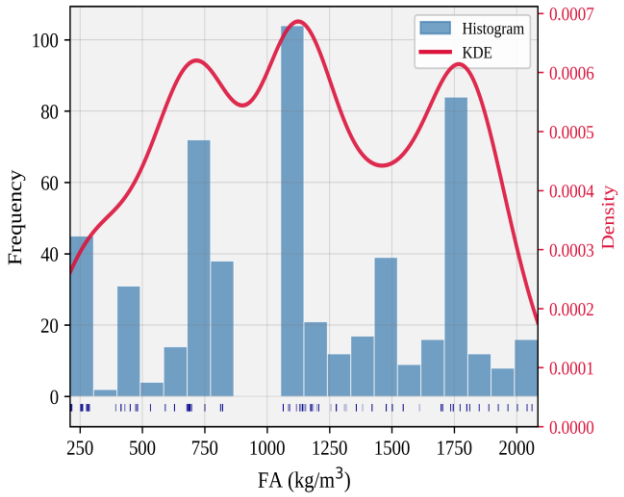




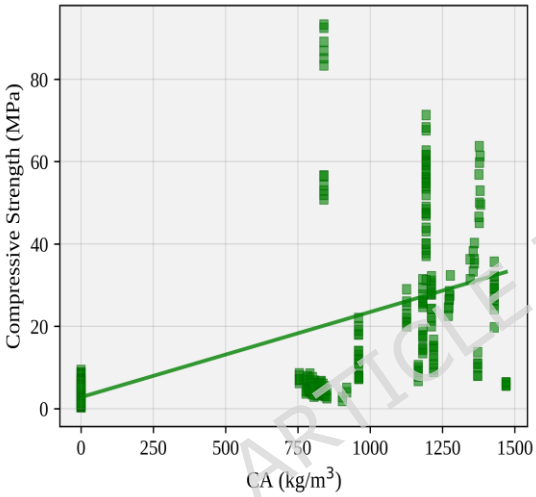
ARTICLE IN PRESS

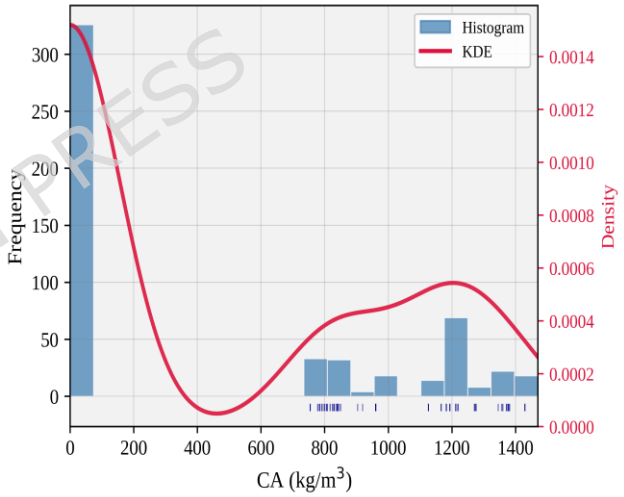
(d)



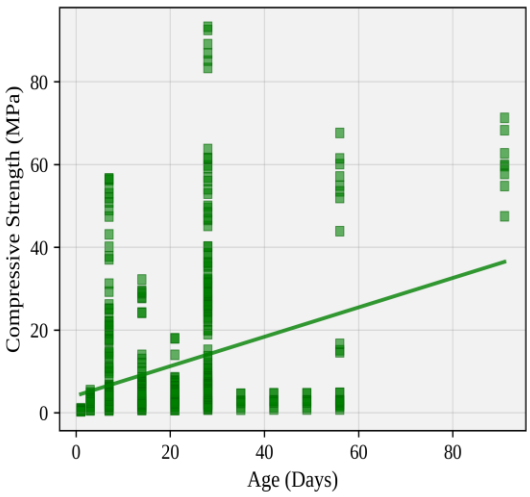


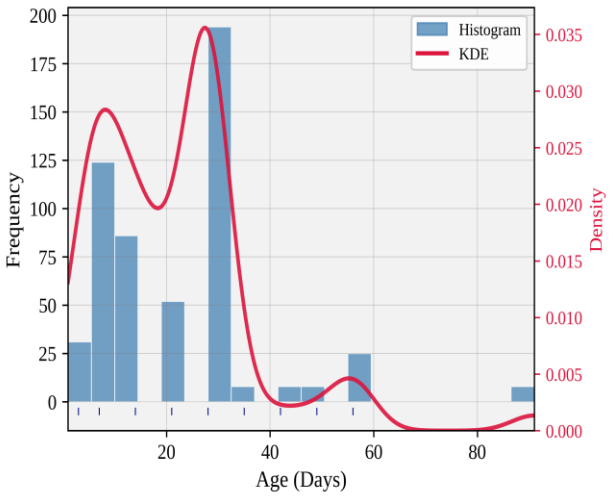
(e)





(f)





ARTICLE IN PRESS

ARTICLE IN PRESS

Fig. 3. Variation in Compressive Strength of HCB with respect to (a) W/C, (b) RA (kg/m^3), (c) Binder (kg/m^3), (d) FA (kg/m^3), (e) CA (kg/m^3), and (f) Curing age (Days).

To systematically characterize the linear interdependencies among all predictor variables and the target response, a Pearson correlation matrix was computed and is reported in **Table 2**, with the corresponding lower-triangular heatmap presented in **Fig. 4**, where both circle size and color intensity encode the magnitude and directionality of each pairwise coefficient. Among the input-output relationships, coarse aggregate content yielded the strongest positive correlation with compressive strength (r = 0.66), affirming its dominant contribution to mechanical performance in HCB systems, followed by binder content (r = 0.39) and curing age (r = 0.32), the latter reflecting the logarithmic strength gain associated with progressive cement hydration. Fine aggregate content exhibited a moderate negative correlation (r = −0.36), consistent with the dilution effect of high sand volumes on binder efficiency, while W/C ratio demonstrated an inverse relationship (r = −0.26) in accordance with the classical Abrams' law. Recycled aggregate content registered the weakest correlation with compressive strength (r = −0.13), suggesting that its influence on mechanical performance is highly conditional on concurrent mix design parameters rather than operating as an independent determinant. Among inter-predictor relationships, the strong negative covariance between FA and CA (r = −0.77), prominently visualized as a deep blue circle in **Fig. 4,** indicates a systematic inverse substitution between fine and coarse aggregate constituents across the compiled mix designs, reflecting the volumetric constraints inherent to aggregate proportioning. The moderate positive correlation between W/C and FA (r = 0.47) and the corresponding negative association between W/C and CA (r = −0.43) further reveal compositional interdependencies that underscore the need to employ nonlinear ensemble modelling to capture multicollinear interactions, rather than relying on univariate or linear regression frameworks. **Table 3** shows final hyperparameter values for all six models, and the approximate computation time on a standard laptop (Intel Core i7, 16 GB RAM) was 2–8 minutes per model.

ARTICLE IN PRESS

Table 2: Correlation Matrix of Input Variables

Variables		Input						Output Parameter
		RA (kg/m^3)	W/C	Binder (kg/m^3)	FA (kg/m^3)	CA (kg/m^3)	Age (Days)	Compressive Strength (MPa)
Input	RA (kg/m^3)	1	–	–	–	–	–	–
	W/C	0.32	1	–	–	–	–	–
	Binder (kg/m^3)	0.23	-0.15	1	–	–	–	–
	FA (kg/m^3)	0.01	0.47	0.04	1	–	–	–
	CA (kg/m^3)	-0.10	-0.43	0.25	-0.77	1	–	–
	Age (Days)	0.15	0.14	0.2	0.03	0.09	1	–
Output	Compressive Strength (MPa)	-0.13	-0.26	0.39	-0.36	0.66	0.32	1

ARTICLE IN PRESS

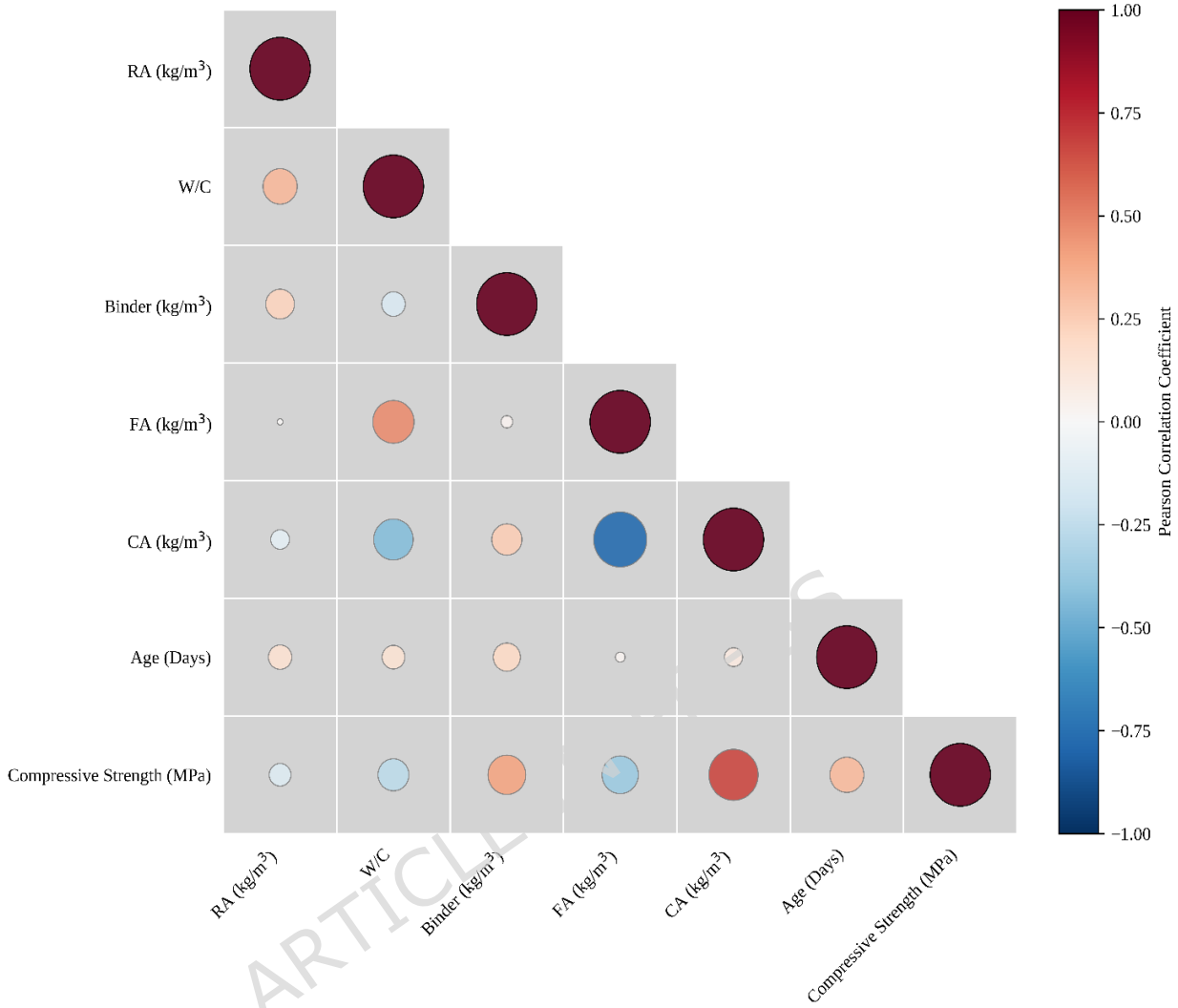


Figure 4. Correlation matrix heat map of the Input variables.

Table 3. Hyperparameter values of the proposed Hybrid Machine Learning models.

Model	Component	Parameter	Value
HSE	Random Forest	n_estimators	300
		random_state	42
	XGBoost	n_estimators	400
		learning_rate	0.05
		max_depth	6
		subsample	0.9
		colsample_bytree	0.9
	ANN	hidden_layer_sizes	(128, 64)
		activation	relu
		solver	adam
		max_iter	1000

ARTICLE IN PRESS

HRL	Meta-Learner	type	Ridge
		alpha	1
	Base Model (XGBoost)	n_estimators	450
		learning_rate	0.05
		max_depth	6
		subsample	0.9
		colsample_bytree	0.9
	Residual Model (ANN)	hidden_layer_sizes	(128, 64)
		activation	relu
		solver	adam
		max_iter	1000
HWE	LightGBM	n_estimators	400
		learning_rate	0.05
		max_depth	6
		num_leaves	31
	XGBoost	n_estimators	400
		learning_rate	0.05
		max_depth	6
		subsample	0.9
	CatBoost	iterations	400
		learning_rate	0.05
		depth	6
	Ensemble	weight_optimization	SLSQP
HML	Random Forest	n_estimators	300
		max_depth	15
		min_samples_split	5
	XGBoost	n_estimators	300
		learning_rate	0.05
		max_depth	6
	LightGBM	n_estimators	300
		learning_rate	0.05
	CatBoost	iterations	300
		learning_rate	0.05
HBS	Meta-Learner	type	Ridge
		alpha	1
	Random Forest	n_estimators	250
		max_depth	15
	Gradient Boosting	n_estimators	250
		learning_rate	0.05
		max_depth	5
	XGBoost	n_estimators	250
		learning_rate	0.05
		max_depth	6
	Meta-Learner	type	BayesianRidge

ARTICLE IN PRESS

ARTICLE IN PRESS

		max_iter	300
		tol	1.00E-03
		alpha_1	1.00E-06
	Random Forest	n_estimators	300
		max_depth	12
		n_estimators	300
HFF	XGBoost	learning_rate	0.05
		max_depth	6
	Meta-Learner	type	Ridge
		alpha	1

2.5. Data preprocessing

The integrity and quality of input data fundamentally determine the reliability and accuracy of machine learning predictions. Raw experimental data from multiple research sources inevitably contain inconsistencies, missing values, and formatting irregularities that must be systematically addressed before model development. This study implements a comprehensive preprocessing pipeline to transform heterogeneous concrete mixture data into a standardized format suitable for hybrid ensemble learning algorithms. All preprocessing transformations are stored in serialized pipeline objects to ensure identical processing of new data during model deployment. This systematic preprocessing framework establishes a robust foundation for the subsequent development of hybrid ensemble models and ensures that machine learning algorithms receive clean, consistent, and properly scaled inputs, maximizing predictive accuracy while maintaining physical interpretability.

2.5.1. Hybrid Stacked Ensemble (HSE)

The Hybrid Stacked Ensemble represents a two-level hierarchical learning architecture that combines heterogeneous base learners through a meta-learning layer. The HSE architecture comprises three base learners selected for their algorithmic diversity and proven performance in regression tasks. Random Forest (RF) provides robust ensemble predictions through bootstrap aggregation and random feature subsampling. Extreme Gradient Boosting (XGB) serves as the second base learner, implementing gradient boosted decision trees with advanced regularization techniques. The third base learner is a Multi-Layer Perceptron (MLP) neural network with an architecture of $[9 \rightarrow 128 \rightarrow 64 \rightarrow 1]$, where 9 represents the input feature dimension, and 1 denotes the single output (compressive strength). Mathematically, the HSE prediction for input x is expressed as:

$$\hat{y}_HSE(x) = w_0 + w_1 \cdot RF(x) + w_2 \cdot XGB(x) + w_3 \cdot MLP(x) + \lambda \cdot ||w||^2 \quad (1)$$

where RF(x), XGB(x), and MLP(x) represent predictions from the three base models, w_0 is the intercept term, w_1, w_2, w_3 are learned weights, and $\lambda \cdot ||w||^2$ is the L2 regularization penalty with $\lambda = 1.0$. The weights are optimized through ridge regression to minimize validation error while penalizing large coefficient magnitudes.

ARTICLE IN PRESS

2.5.2. Hybrid Residual Learning (HRL)

The Hybrid Residual Learning architecture implements a sequential correction strategy where a secondary model learns to predict and compensate for the systematic errors produced by a primary base model, XGB. This configuration yields robust initial predictions by capturing the dominant nonlinear relationships between concrete mixture parameters and compressive strength. However, even well-tuned gradient boosting models exhibit systematic prediction biases for certain mixture compositions or strength ranges. After training the XGB base model on the training set, residuals are computed as:

$$r_i = y_i - \hat{y}_{XGB}(x_i) \quad (2)$$

where y_i represents the true compressive strength of the i-th training sample, $\hat{y}_{XGB}(x_i)$ is the XGB prediction, and r_i is the resulting residual. These residuals quantify the base model's prediction errors and serve as targets for the secondary residual learner. The residual learner employs an MLP with architecture $[9 \rightarrow 128 \rightarrow 64 \rightarrow 1]$ and ReLU activations, identical to the MLP in HSE. The neural network is trained on the original input features x_i, using residuals r_i as targets, to learn the correction term needed to improve the base model's accuracy. The final HRL prediction combines the base model output with the learned residual correction:

$$\hat{y}_{HRL}(x) = \hat{y}_{XGB}(x) + \hat{y}_{MLP_residual}(x) \quad (3)$$

This additive formulation ensures that the residual network focuses exclusively on modeling systematic errors rather than re-learning patterns already captured by XGB. The heterogeneity between tree-based (XGB) and neural network (MLP) architectures is crucial, as the neural network can model smooth, non-linear error patterns that gradient-boosted trees may miss due to their piecewise-constant predictions.

2.5.3. Hybrid Weighted Ensemble (HWE)

The Hybrid Weighted Ensemble implements adaptive weighted averaging of three state-of-the-art gradient boosting algorithms, with weights optimized through numerical minimization on training data. Unlike simple averaging or voting ensembles, HWE learns data-driven combination weights that reflect each base model's relative predictive strength for concrete compressive strength. Each base model is independently trained on the full training set, producing predictions $p_{LGBM}(x)$, $p_{XGB}(x)$, and $p_{CB}(x)$ for any input x. The ensemble prediction is computed as:

$$\hat{y}_{HWE}(x) = w_1 \cdot p_{LGBM}(x) + w_2 \cdot p_{XGB}(x) + w_3 \cdot p_{CB}(x) \quad (4)$$

subject to the constraint $w_1 + w_2 + w_3 = 1$ and $w_i \geq 0$ for all i, ensuring non-negative normalized weights that sum to unity. Optimal weights are determined through Sequential Least Squares Programming (SLSQP), a gradient-based optimization algorithm that minimizes the mean squared error between ensemble predictions and true values on the training set. The objective function is:

$$\text{minimize}_w \ (1/n) \cdot \Sigma_i [y_i - (w_1 \cdot p_{LGBM}(x_i) + w_2 \cdot p_{XGB}(x_i) + w_3 \cdot p_{CB}(x_i))]^2 \quad (5)$$

ARTICLE IN PRESS

subject to: $w_1 + w_2 + w_3 = 1$, $w_1 \geq 0$, $w_2 \geq 0$, $w_3 \geq 0$. The data-driven weight optimization distinguishes HWE from fixed-weight ensembles and allows the model to automatically adapt to the relative strengths of each base learner for the specific, concrete strength prediction task. If one algorithm consistently outperforms others, its weight increases accordingly. Conversely, if all three models perform similarly, weights approach equal distribution, approximating simple averaging.

2.5.4. Hybrid Meta-Learning (HML)

The Hybrid Meta-Learning architecture extends stacked generalization by combining original input features with meta-features derived from diverse base models, enabling the meta-learner to leverage both raw material properties and high-level patterns recognized by base learners. This dual information source enhances predictive accuracy by providing the meta-learner with richer context for estimating compressive strength.

Four diverse base models constitute the first learning level, each employing distinct algorithmic principles to maximize ensemble diversity. Each base model is trained independently on the training set, and its predictions on both the training and test sets are used to compute meta-features. For the i-th training sample with original features x_i, the augmented feature representation becomes:

$$x_i^{(meta)} = [x_i, p_RF(x_i), p_XGB(x_i), p_LGBM(x_i), p_CB(x_i)] \quad (6)$$

where the augmented feature vector concatenates the 9 original features with 4 meta-features representing base model predictions, yielding a 13-dimensional representation. This augmentation provides the meta-learner with both raw concrete composition data and high-level abstractions learned by diverse algorithms. Mathematically, the HML prediction is:

$$\hat{y}_HML(x) = w_0 + \Sigma_{j=1}^{9} \beta_j \cdot x_j + \Sigma_{k=1}^{4} \gamma_k \cdot p_k(x) + \lambda \cdot (||\beta||^2 + ||\gamma||^2) \quad (7)$$

where β_j are coefficients for original features, γ_k are coefficients for meta-features (base model predictions), w_0 is the intercept, and $\lambda = 1.0$ controls regularization strength. This approach guarantees that HML performance estimates accurately reflect real-world application scenarios.

2.5.5. Hybrid Bayesian Stacking (HBS)

The Hybrid Bayesian Stacking architecture implements a probabilistic meta-learning framework that quantifies prediction uncertainty while combining base learner outputs. Unlike deterministic meta-learners (Ridge, ordinary least squares), Bayesian Ridge regression maintains probability distributions over meta-learner coefficients, providing principled uncertainty quantification for ensemble predictions. The Bayesian framework learns not only point estimates for meta-learner coefficients but also their posterior uncertainties, quantifying confidence in the learned combination weights. The Bayesian Ridge meta-learner produces predictions as:

$$\hat{y}_HBS(x) = w_0 + w_1 \cdot p_RF(x) + w_2 \cdot p_GB(x) + w_3 \cdot p_XGB(x) \quad (8)$$

ARTICLE IN PRESS

where weights $w = [w_0, w_1, w_2, w_3]$ are drawn from learned posterior distributions rather than being fixed point estimates. This probabilistic treatment enables uncertainty quantification: predictions come with credible intervals reflecting both model uncertainty (epistemic) and data noise (aleatoric).

2.5.6. Hybrid Feature Fusion (HFF)

The Hybrid Feature Fusion architecture transforms the original feature space via dimensionality reduction before ensemble learning, yielding a richer representation that combines original features with principal components capturing dominant directions of variance. This approach addresses potential redundancy in the original feature set while preserving essential information through principled dimensionality reduction.

Feature fusion begins with standardization of all nine input features to zero mean and unit variance, ensuring that PCA identifies variance directions based on correlation structure rather than measurement scales. Principal Component Analysis (PCA) is then applied to the standardized training features, extracting the top 5 principal components that capture the dominant directions of variance in the concrete mixture data. The PCA transformation computes eigenvectors $v_1, v_2, ..., v_5$ of the feature correlation matrix, ordered by decreasing eigenvalues $\lambda_1 \geq \lambda_2 \geq ... \geq \lambda_5$. For each training sample x_i, the principal component scores are:

$$PC_k(x_i) = \Sigma_{j=1}^{9} v_kj \cdot (x_ij - \mu_j) / \sigma_j \quad (9)$$

where $k \in \{1,2,3,4,5\}$, v_kj is the j-th element of the k-th eigenvector, x_ij is the j-th feature value, and μ_j, σ_j are the mean and standard deviation of feature j. The five principal components typically explain 85-95% of total variance, providing a compact representation of the primary variation patterns in concrete mixture compositions. The fused feature representation concatenates standardized original features with principal component scores:

$$x_i\text{^(fused)} = [x_i\text{^(std)}, PC_1(x_i), PC_2(x_i), PC_3(x_i), PC_4(x_i), PC_5(x_i)] \quad (10)$$

The meta-learning layer employs Ridge regression ($\alpha = 1.0$) to combine predictions from the two base models trained on fused features. The meta-learner is trained on stacked predictions, following the same two-phase protocol as HSE, to learn optimal combination weights for the RF and XGB predictions derived from fused features.

2.6. Model Training and Hyperparameter Optimization

All six hybrid models were trained using a systematic protocol designed to maximize predictive accuracy, prevent overfitting, and ensure reproducibility. The training set was used exclusively for model fitting, the validation set for hyperparameter selection and early stopping, and the test set for final performance evaluation, as reported in the results.

Hyperparameter optimization employed grid search with 5-fold cross-validation on the training set. For each hyperparameter configuration, the training set was divided into 5 folds, and models were trained on 4 folds while evaluating on the held-out fold. This process was repeated 5 times

ARTICLE IN PRESS

with different held-out folds, and the average validation performance was used to determine the score for each configuration. The configuration achieving the best cross-validation score was selected as the final hyperparameter set. All hyperparameter details are attached in **Table 3**.

2.7. SHAP Analysis

SHAP (SHapley Additive exPlanations) interprets a model output by breaking it down into a baseline value plus separate contributions from each input variable. For a prediction $f(x)$ with M features, SHAP represents the model as-

$$f(x) = \phi_0 + \sum_{j=1}^{M} \phi_j \tag{11}$$

where ϕ_0 is the average prediction over all samples, and ϕ_j quantifies how much of a feature j increases or decreases the prediction for that particular instance relative to the baseline. In practice, these contributions are calculated using Shapley theory by averaging the marginal impact of a feature across many different subsets of the remaining features [77].

2.8. Uncertainty Analysis

Uncertainty analysis evaluates how reliable a model's predictions are by assigning a numerical measure to the spread or variability of possible outputs for a given input. In regression, the predictive distribution $p(y \mid x)$ is often summarized by its variance,

$$\mathrm{Var}(y \mid x) = \mathbb{E}[y^2 \mid x] - (\mathbb{E}[y \mid x])^2 \tag{12}$$

where $\mathbb{E}[y \mid x]$ is the predicted mean response, and $\mathrm{Var}(y \mid x)$ expresses the dispersion around that mean. This variance can be obtained from Bayesian models, ensembles, or resampling-based frameworks, and it helps distinguish between regions of the input space where the model is confident and regions with high predictive risk [78].

ARTICLE IN PRESS

ARTICLE IN PRESS

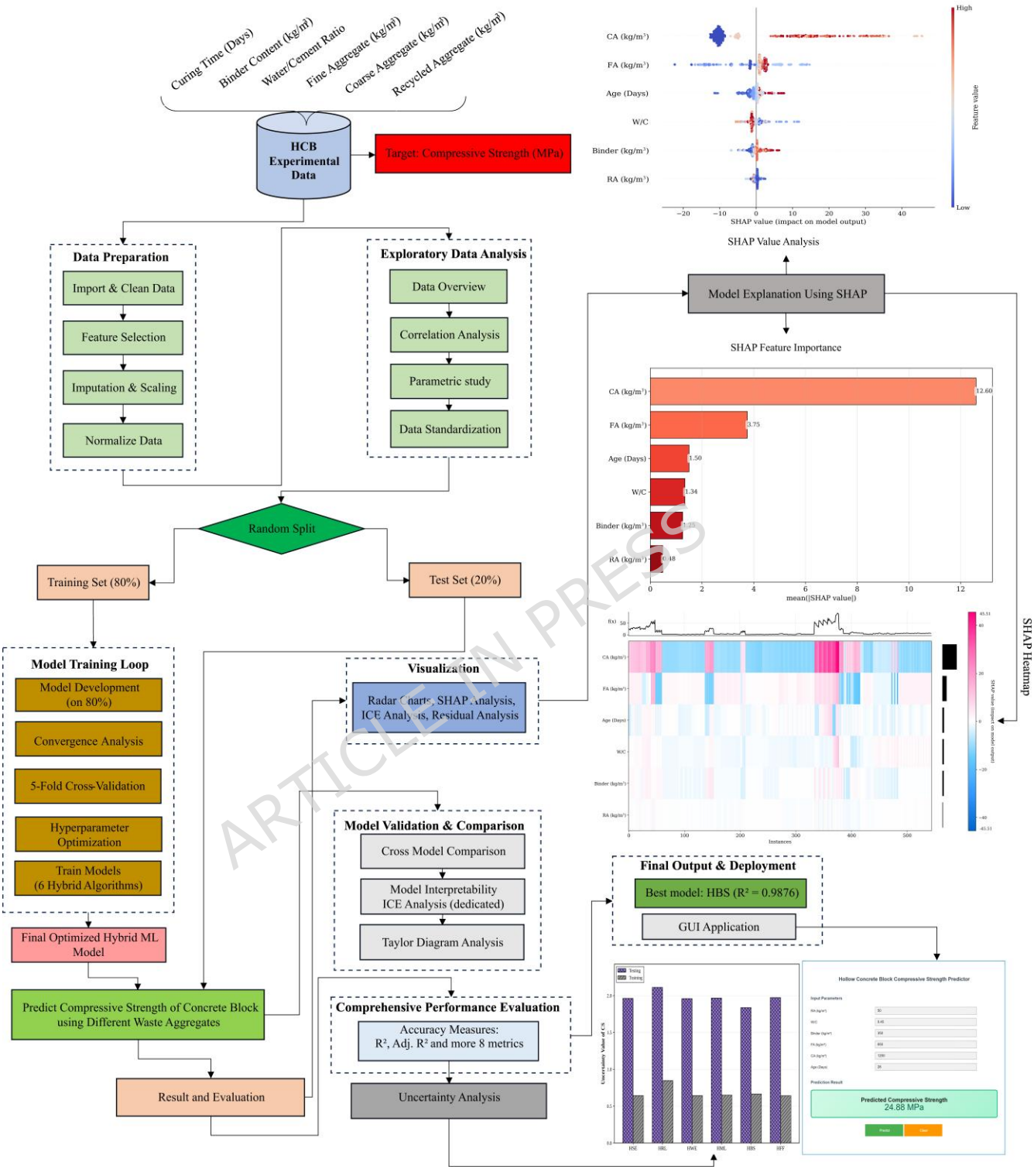


Figure 5. Visual representation of the process for Hybrid ML models

ARTICLE IN PRESS

2.9. Model Metrics

The evaluation of model performance relies on robust quantitative measurements that rigorously assess prediction accuracy and reliability across a range of testing conditions. The evaluation methodology includes several statistical measures to make sure the model is fully validated: (1) Coefficient of determination (R^2), (2) Mean absolute error (MAE) (3) Scatter Index (SI) (4) Performance Index (PI) (5) Theil's U Statistic (U) (6) t-Statistic (T) (7) Objective Function (OBJ) (8) Scaled RMSE Index (SCI) (9) Explained Variance Score (EVS) [79–84]. All mathematical formulas and the standard range are attached in **Table 4.**

Table 4. Evaluation criteria for performance evaluating the Hybrid ML models.

Name of Goodness Criteria	Expression	Standard Range
Coefficient of Determination (R^2)	$R^2 = 1 - \frac{\sum_{i=1}^{n}(X_i - Y_i)^2}{\sum_{i=1}^{n}(X_i - \bar{u})^2}$	0 – 1
Root Mean Square Error (RMSE)	$\mathrm{RMSE} = \sqrt{\frac{1}{n}\sum_{i=1}^{n}(X_i - Y_i)^2}$	0 is the best value
Scatter Index (SI)	$\mathrm{SI} = \frac{\mathrm{RMSE}}{\bar{u}_{obs}}$	0 is the best value
Performance Index (PI)	$\mathrm{PI} = r \times (1 - \mathrm{SI})$	$(-\infty, 1] \rightarrow 1$ best
Theil's U Statistic (U)	$U = \frac{\sqrt{\mathrm{MSE}}}{\left(\sqrt{\mathrm{mean}(\hat{y}^2)} + \sqrt{\mathrm{mean}(y^2)}\right)}$	$[0, 1] \rightarrow 0$ best
t-Statistic (T)	$T = \sqrt{\frac{(n-2)\cdot R^2}{(1-R^2)}}$	$[0, \infty) \rightarrow$ higher best
Objective Function (OBJ)	$\mathrm{OBJ} = \sqrt{\frac{\left(\frac{\mathrm{RMSE}_{tr}}{\sigma_{tr}}\right)^2 + \left(\frac{\mathrm{RMSE}_{te}}{\sigma_{te}}\right)^2}{2}}$	0 is the best value
Scaled RMSE Index (SCI)	$\mathrm{SCI} = \frac{\mathrm{RMSE}}{\max(y) - \min(y)}$	0 is the best value
Explained Variance Score (EVS)	$\mathrm{EVS} = 1 - \frac{\mathrm{Var}(y - \hat{y})}{\mathrm{Var}(y)}$	$(-\infty, 1] \rightarrow 1$ best

Note: Xi – actual value; Yi – predicted value; ū – mean of actual values; n – sample size; σ – standard deviation; r – Pearson correlation coefficient; ŷ – predicted values; Var(·) – variance operator.

ARTICLE IN PRESS

3. Results and discussion

3.1. Statistical analysis of results

The comparison analysis shows that the machine learning algorithms in **Table 5** for predicting concrete compressive strength exhibit markedly different performance levels. Across the six scenarios, all models generalize strongly, with test R^2 tightly clustered near 0.984–0.988 and RMSE around 1.84–2.11, while training metrics are uniformly higher ($R^2 \approx 0.998$; RMSE ≈ 0.64–0.85), indicating minimal overfitting and stable bias–variance trade-offs. HBS yields the best test-set accuracy ($R^2 = 0.9876$) and the lowest RMSE (1.8363), closely followed by HWE and HSE. In contrast, HRL shows the highest test error (RMSE = 2.1109) within a still-narrow band, making differences practically slight but methodologically notable. The supplementary indices reinforce this ranking: HBS achieves the lowest SIs (0.1648), U (0.0463), OBJ (0.0832), and SCI (0.0273), along with the highest PIs (0.83) and T-stats (92.336), confirming its superior predictive consistency. The parallel trends of these metrics across phases confirm metric consistency, and the miniature train–test gaps across all scenarios suggest a robust preprocessing and tuning pipeline that is resilient to scenario-specific data shifts

Table 5. Description of each model's performance metrics in the training and testing datasets.

Model	Phase	R^2	RMSE	SI	PI	U	T-stat	OBJ	SCI	EVS
HSE	Training	0.9987	0.6431	0.0534	0.9459	0.0151	566.8661	0.088	0.0069	0.9987
	Testing	0.9859	1.9619	0.1761	0.8181	0.0494	86.3497	0.088	0.0292	0.9859
HRL	Training	0.9977	0.8469	0.0704	0.9286	0.0199	430.2553	0.0967	0.0091	0.9977
	Testing	0.9836	2.1109	0.1895	0.8039	0.0531	80.1618	0.0967	0.0314	0.9837
HWE	Training	0.9987	0.6432	0.0534	0.9459	0.0151	566.7704	0.0879	0.0069	0.9987
	Testing	0.9859	1.9587	0.1758	0.8184	0.0493	86.4912	0.0879	0.0291	0.9859
HML	Training	0.9986	0.6491	0.0539	0.9454	0.0153	561.5847	0.0883	0.007	0.9986
	Testing	0.9858	1.9661	0.1764	0.8177	0.0495	86.1645	0.0883	0.0292	0.9858
HBS	Training	0.9986	0.6651	0.0553	0.9441	0.0156	548.1099	0.0832	0.0072	0.9986
	Testing	0.9876	1.8363	0.1648	0.83	0.0463	92.336	0.0832	0.0273	0.9876
HFF	Training	0.9987	0.6414	0.0533	0.9461	0.0151	568.3594	0.0884	0.0069	0.9987
	Testing	0.9857	1.9724	0.177	0.8171	0.0497	85.8848	0.0884	0.0293	0.9857

3.2. Comparison of evaluation criteria of hybrid ML models

Table 6 and **Figure 6** present a comprehensive multi-metric ranking and score analysis of the six hybrid predictive models across nine statistical performance indicators (R^2, RMSE, SI, PI, U, T-

ARTICLE IN PRESS

stat, OBJ, SCI, and EVS) for both training and testing phases, with each model assigned a rank score of 1 to 6 per metric, aggregated into a Total Score and Final Score. The results clearly establish HWE as the top-performing model with the highest Final Score of 92, followed by HSE (86), HBS (78), HFF (68), HML (55), and HRL (18), demonstrating a well-defined performance hierarchy. This ranking is visually corroborated by the radar charts in Figure 6, where the shaded polygons across the training phase (green), testing phase (blue), and combined final score (pink) panels reveal that HWE consistently occupies the outermost positions near the "Best" boundary, while HRL is confined to the innermost region near "Worst," confirming that HWE achieves the most balanced and superior generalization performance across all evaluated statistical criteria.

Table 6. Multi-Metric Ranking and Score Analysis of Hybrid Predictive Models.

Model	Phase	R^2	RMSE	SI	PI	U	T-stat	OBJ	SCI	EVS	Total Score	Final Score
HWE	Training	6	4	5	5	6	4	5	6	6	47	92
	Testing	5	5	5	5	5	5	5	5	5	45	92
HSE	Testing	5	4	4	4	4	4	4	4	5	38	86
	Training	6	5	5	5	6	5	4	6	6	48	86
HBS	Testing	6	6	6	6	6	6	6	6	6	54	78
	Training	3	2	2	2	2	2	6	2	3	24	78
HFF	Testing	2	2	2	2	2	2	2	2	2	18	68
	Training	6	6	6	6	6	6	2	6	6	50	68
HML	Testing	3	3	3	3	3	3	3	4	3	28	55
	Training	3	3	3	3	3	3	3	3	3	27	55
HRL	Training	1	1	1	1	1	1	1	1	1	9	18
	Testing	1	1	1	1	1	1	1	1	1	9	18

ARTICLE IN PRESS

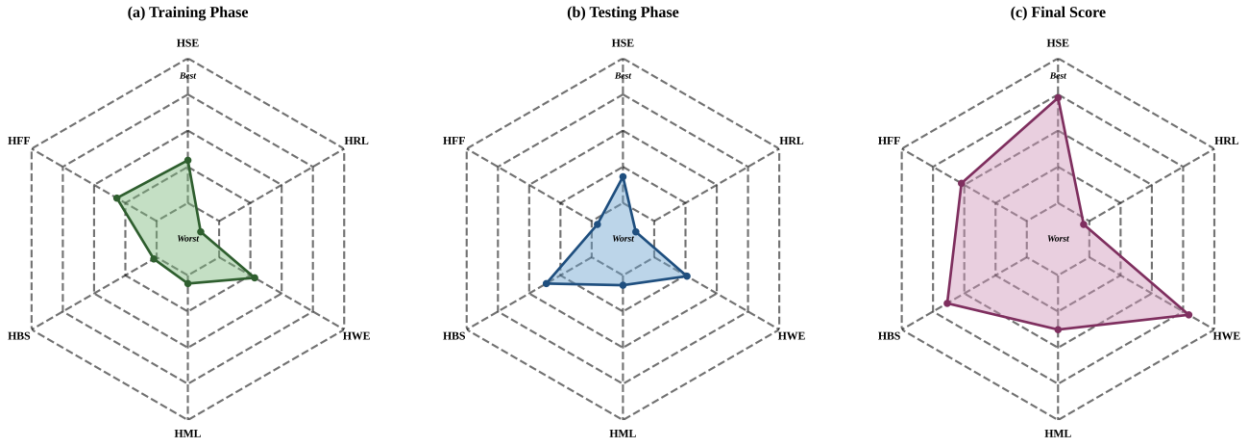
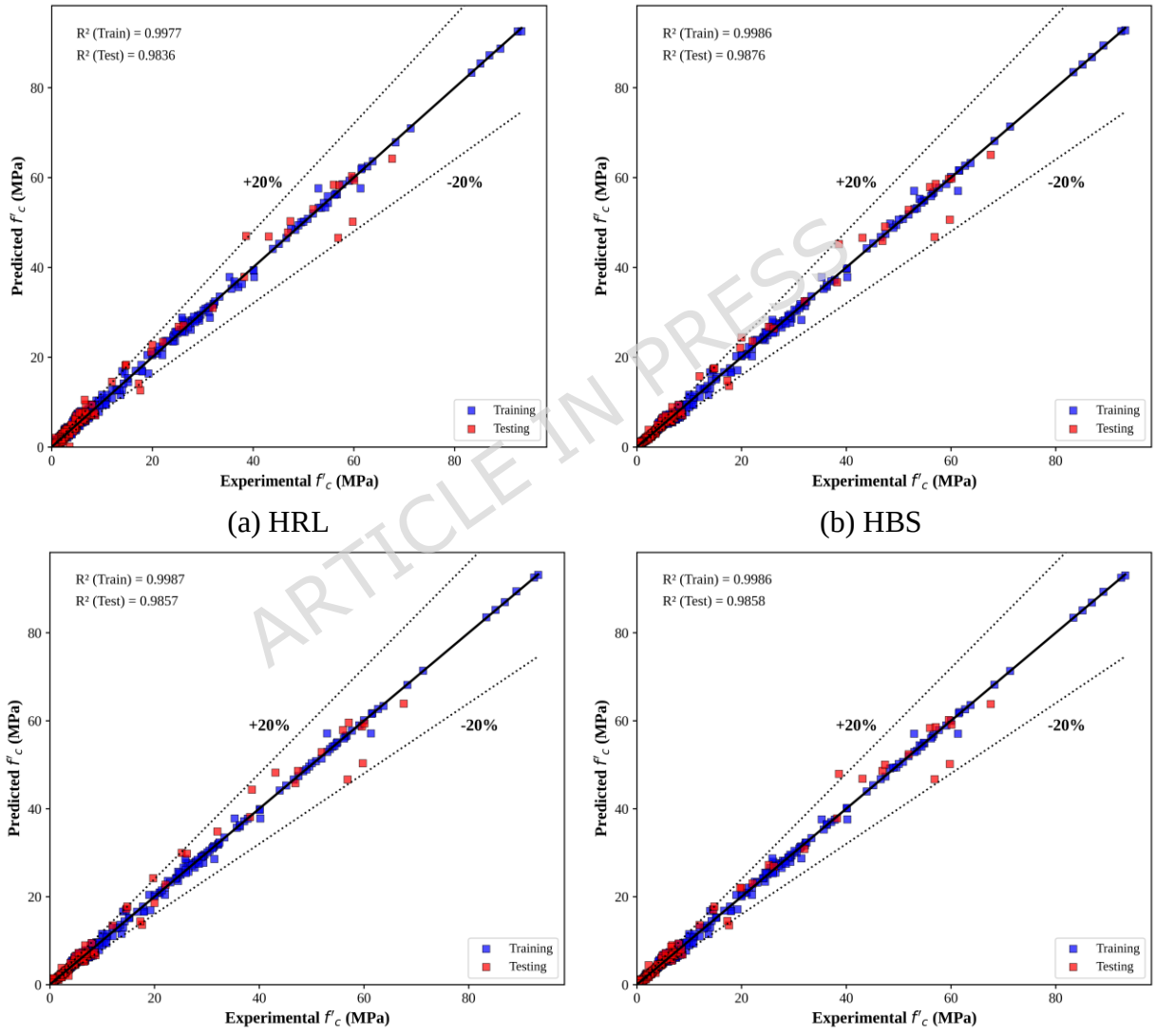


Figure 6: Comparison of hybrid ML model's evaluation metrics based on Radar Chart.

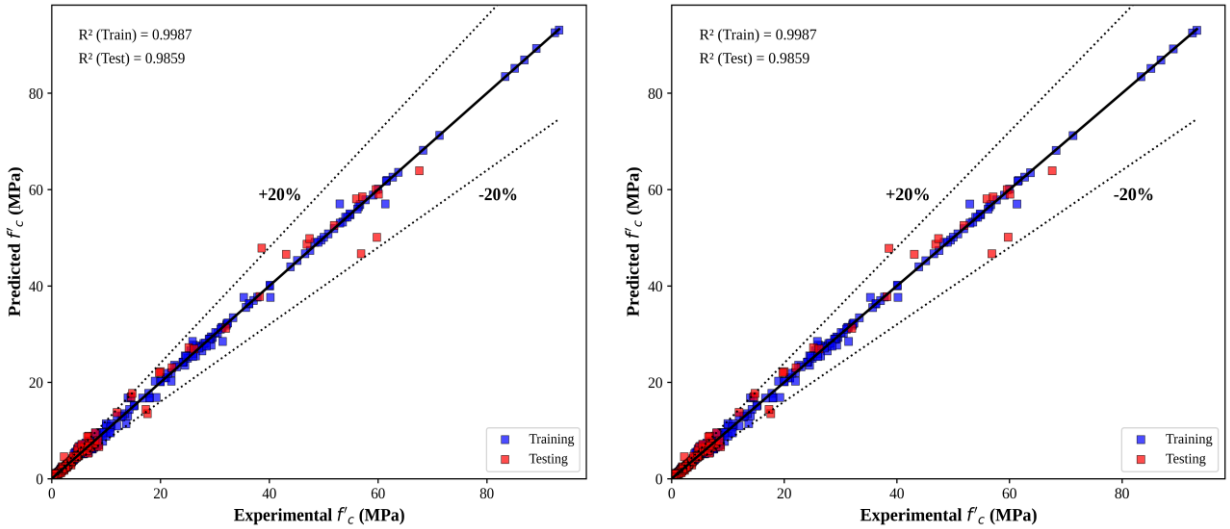
ARTICLE IN PRESS

3.3. Hybrid ML models' prediction performance

Figure 7 illustrates the parity plots of experimental versus predicted compressive strength for the six hybrid ML configurations (HRL, HBS, HFF, HML, HSE, and HWE) in both training and testing phases, together with the ±20% error bands. All models exhibit near-unity linear trends, with R^2 values above 0.98 in training and approximately 0.984–0.988 in testing. HBS and HML show the tightest clustering of points around the 1:1 line and thus are the top performers. In contrast, HRL displays the largest scatter and lowest test R^2, indicating comparatively poorer predictive accuracy among the examined scenarios.



ARTICLE IN PRESS



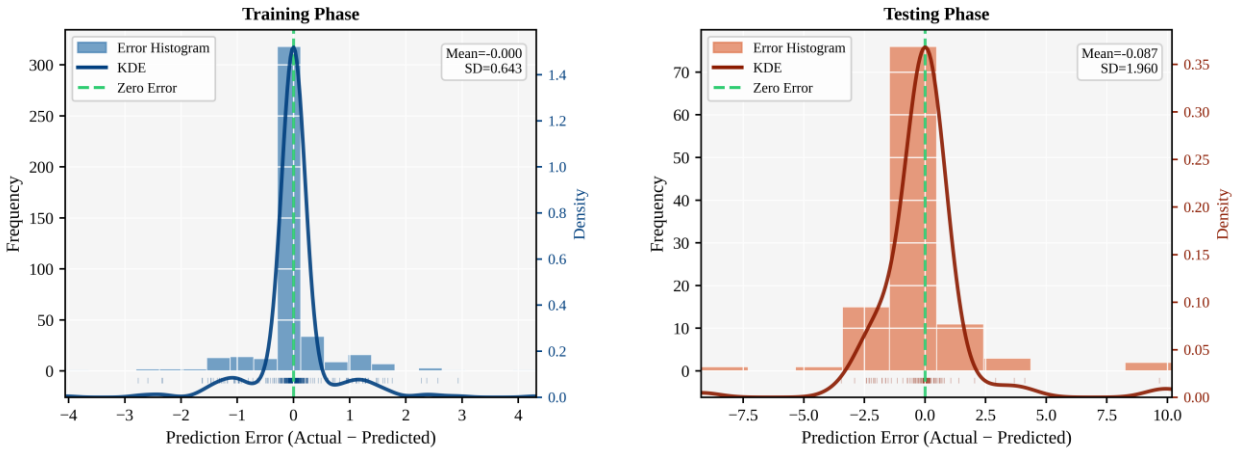
(e) HSE (f) HWE

Figure 7: The scatter plot shows observed vs predicted values of the Hybrid ML models for CS in both phases.

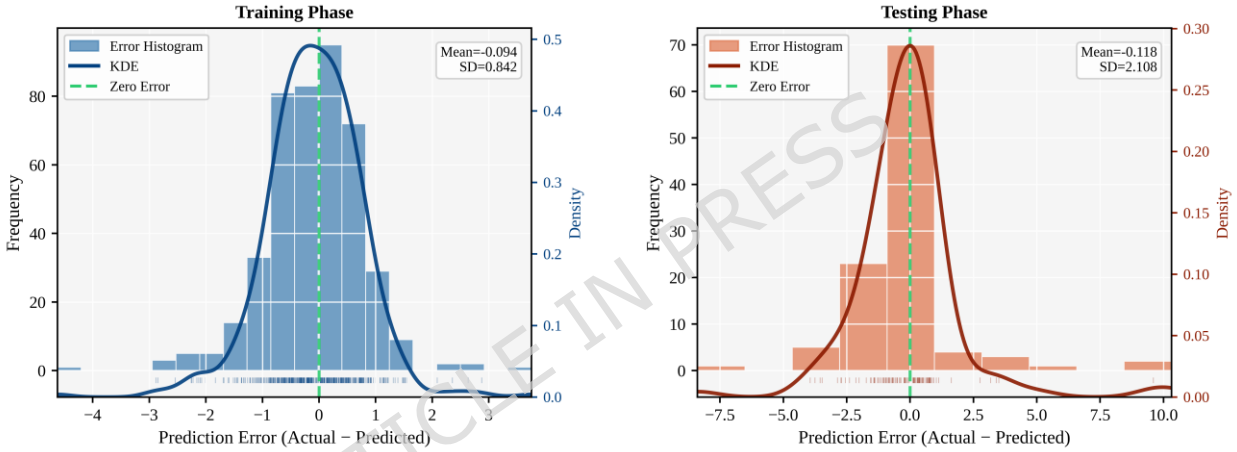
The error histograms with overlaid KDE curves in **Figure 8** show the distribution of prediction errors (Actual − Predicted) for each hybrid model, presented separately for the training and testing phases. In the training phase, all models yield highly concentrated error distributions centered at or near zero, with mean errors essentially zero (≈ −0.094 to +0.004 MPa) and standard deviations within 0.641–0.842 MPa, indicating negligible bias and tight residual spreads. The KDE curves are sharply peaked at zero error, with the majority of training residuals lying within ±1 MPa and the extreme tails confined to approximately ±3 MPa. In the testing phase, the error distributions remain approximately zero-centered (mean errors between −0.118 and −0.053 MPa) but become broader, with standard deviations ranging from 1.835 to 2.108 MPa. Most testing residuals lie within ±2.5 MPa, while a small number of outliers extend up to about 10 MPa, consistent with the moderate increases in test RMSE and MAE reported in Table 5. Among the six configurations, HBS exhibits the lowest testing standard deviation (1.835 MPa) and the narrowest residual spread, whereas HRL shows the highest testing standard deviation (2.108 MPa) and the widest dispersion in both phases. This confirms that HBS is the best-performing model and HRL is the weakest within an overall high-accuracy framework.

ARTICLE IN PRESS

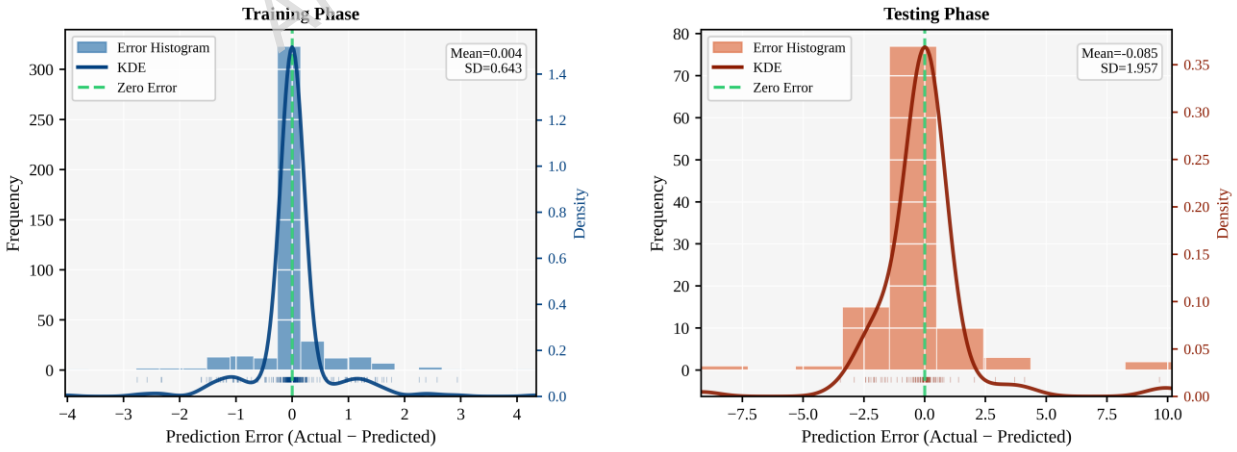
(a) Hybrid Stacked Ensemble (HSE)



(b) Hybrid Residual Learning (HRL)



(c) Hybrid Weighted Ensemble (HWE)



ARTICLE IN PRESS

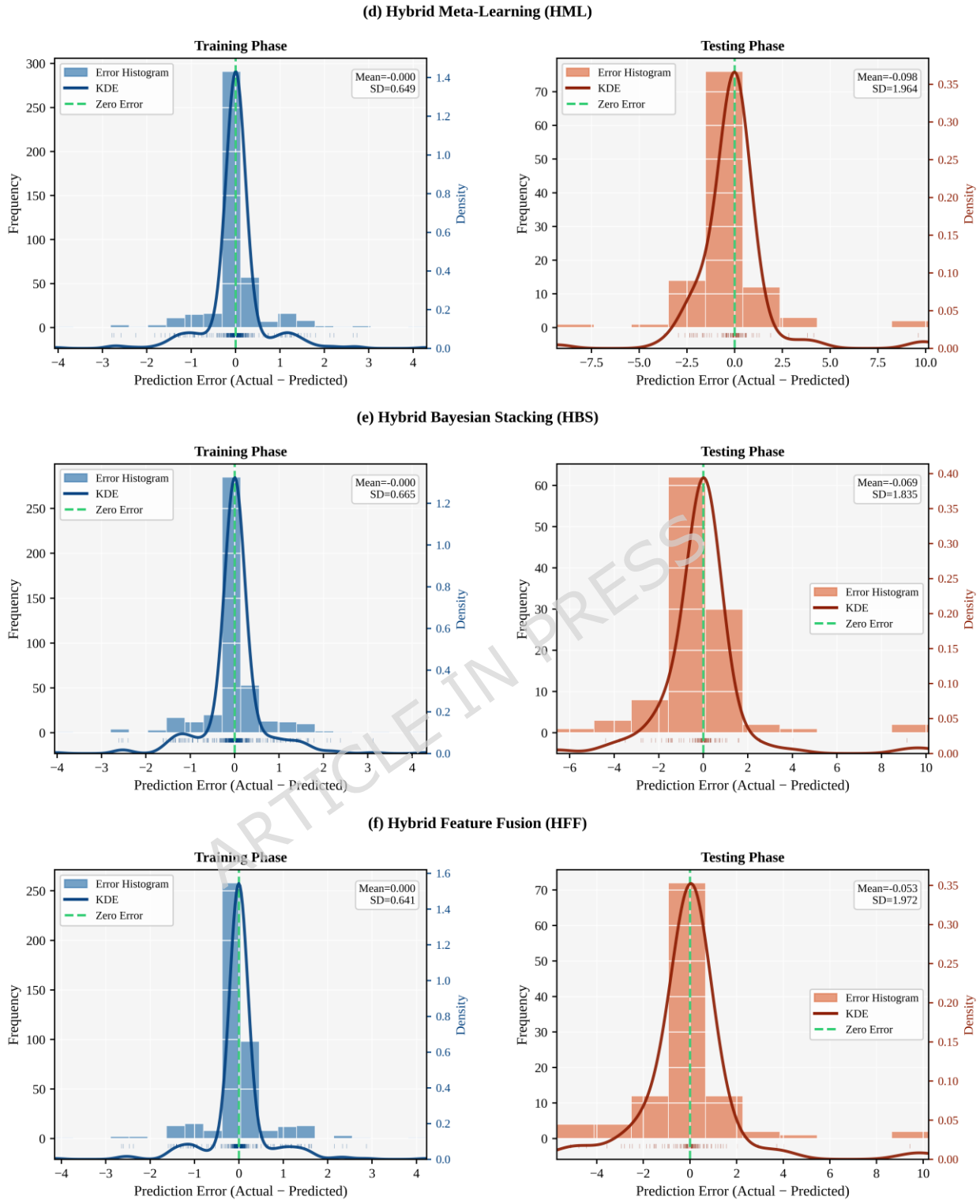
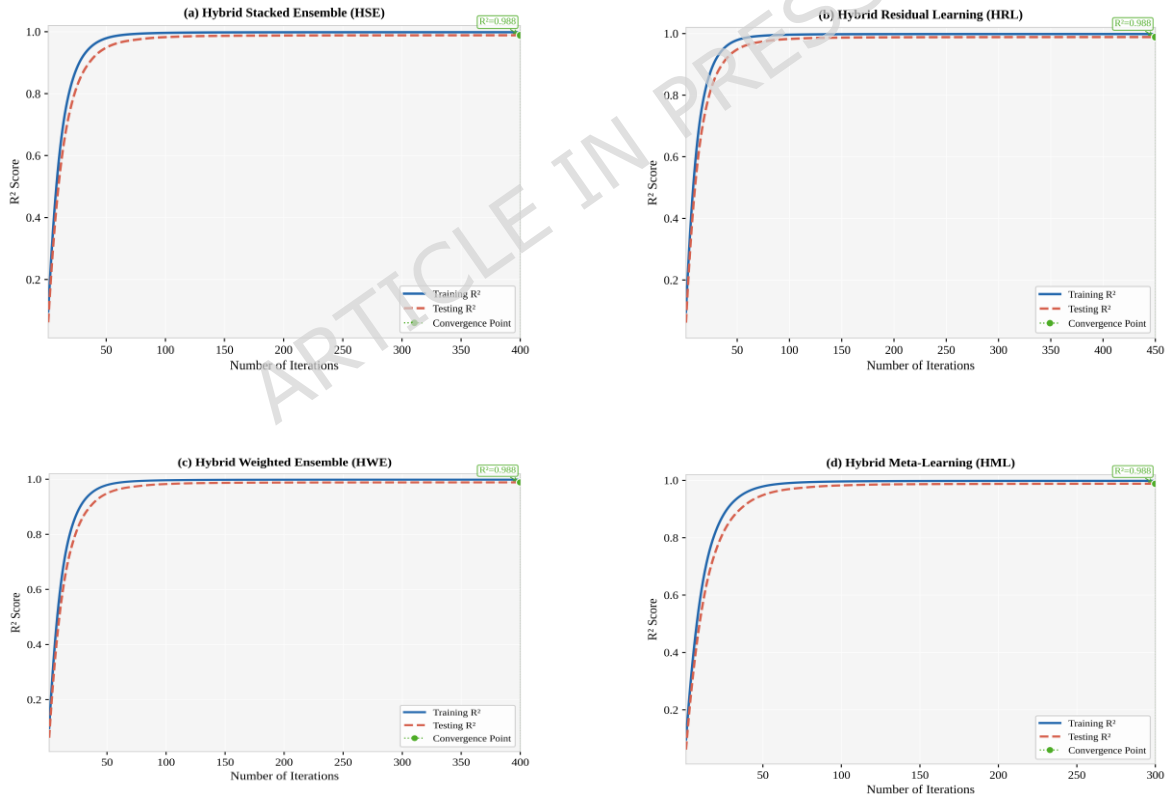


Figure 8: Observed and Predicted values distribution for the Hybrid ML model (both test and training phase).

ARTICLE IN PRESS

3.4. Convergence behaviour of hybrid ML models

Figure 9 illustrates the fitness convergence curves for the six hybrid ML models in terms of R^2 values, showing both training (solid blue) and testing (dashed red) trajectories as a function of the number of iterations. The convergence behaviour across all models reveals a consistent three-phase pattern: a steep ascent during the first 25 iterations, where R^2 rises from approximately 0.10 to 0.90; a gradual stabilisation phase between 25 and 100 iterations; and a final plateau region beyond 100 iterations, where additional iterations yield negligible improvement. The training R^2 curves consistently rise above the testing R^2 curves and approach unity at convergence, while the annotated convergence points indicate testing R^2 values of 0.988 for HSE, HRL, HWE, HML, and HFF, and 0.983 for HBS. The required number of iterations to reach convergence varies among the models, with HBS achieving stable performance in only 250 iterations, followed by HML and HFF (300 iterations), HSE and HWE (400 iterations), and HRL requiring the highest count of 450 iterations. This indicates that HBS exhibits the most efficient convergence, reaching its optimal predictive capacity with the fewest iterations, whereas HRL demonstrates a comparatively slower convergence rate. The training and testing curves remain closest in HSE, HWE, and HFF, indicating minimal divergence between the two phases, whereas HBS and HML show a slightly wider gap during the early iterations before merging at the plateau region.



ARTICLE IN PRESS

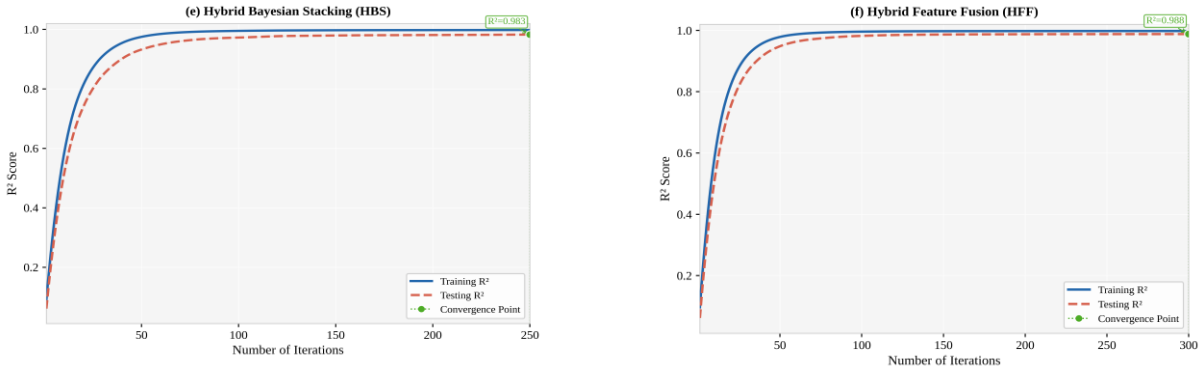


Figure 9. Fitness convergence curves of the hybrid ML model with respect to R^2 values.

3.5. Taylor diagram analysis of hybrid ML models

Figure 10 presents the Taylor diagram analysis of the six developed hybrid ML models, evaluated separately for the training (left) and testing (right) phases against the experimental reference point (black star). In both phases, all six model markers cluster tightly around the reference, with correlation coefficients between 0.95 and 0.99 and standard deviations closely matching those of the observed data (~17 in training and ~16.5 in testing). During training, the markers sit just above the reference at a centred RMSE near the 6.0 contour, indicating near-perfect agreement between predicted and observed values. In the testing phase, the markers shift slightly upward and lie near the 5.0-centred RMSE contour, reflecting the expected reduction in predictive accuracy on unseen data. The compact clustering of all six models across both phases confirms consistent variance reproduction and high correlation, with HBS remaining closest to the reference, as indicated by its lowest test RMSE reported in Table 5.

ARTICLE IN PRESS

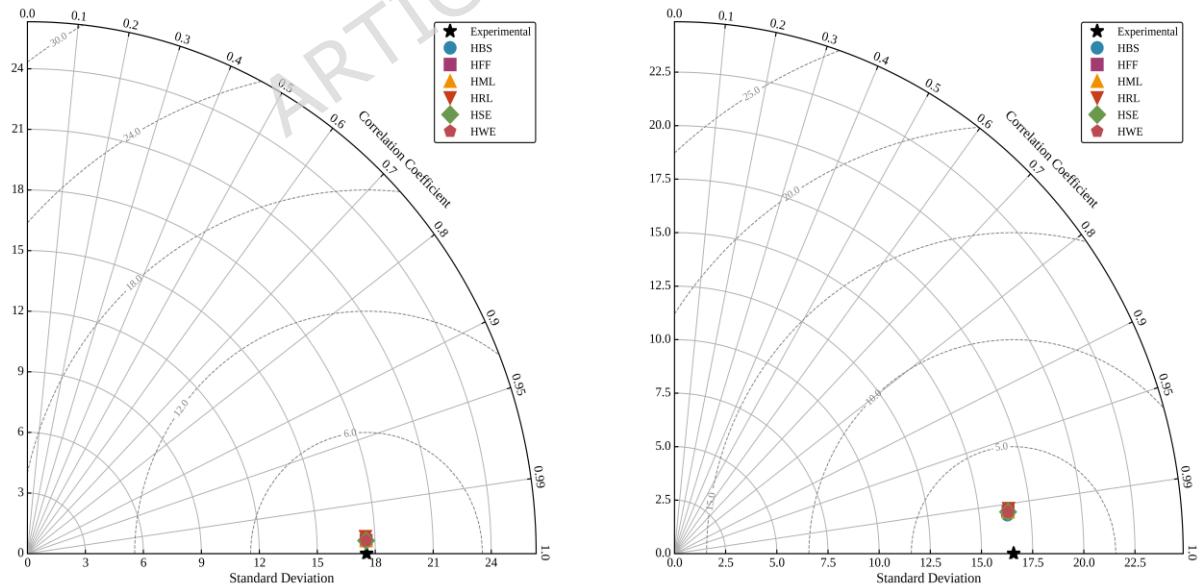


Figure 10. Taylor diagram analysis of the developed 6 hybrid ML models

ARTICLE IN PRESS

3.6. Shapley Additive Explanations (SHAP) analysis

A model-interpretability method called SHAP (Shapley Additive Explanations) analysis describes the direction and magnitude of each input feature's contribution to a machine learning prediction. Each feature is assigned a numerical value by SHAP that indicates how much it influences a prediction relative to a baseline, such as the model's average prediction. When a feature has a positive SHAP value, the predicted output increases; when it has a negative value, the predicted output decreases.

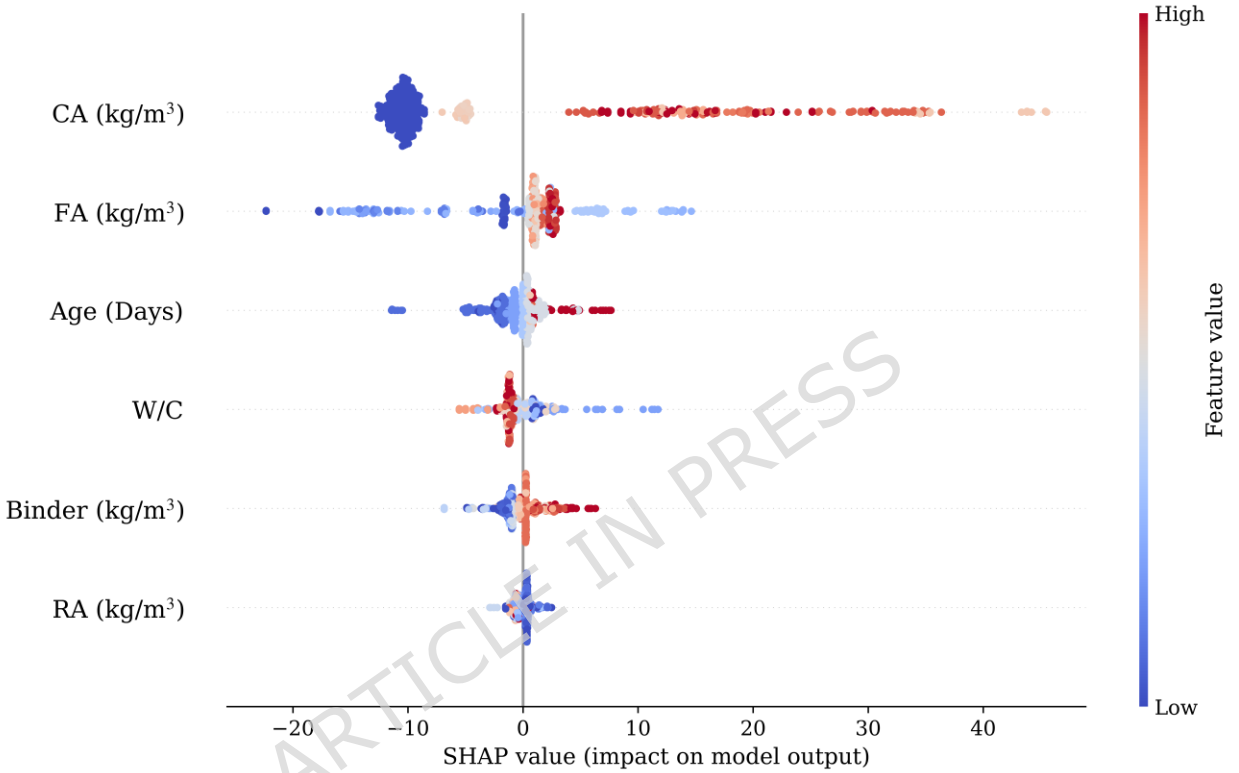
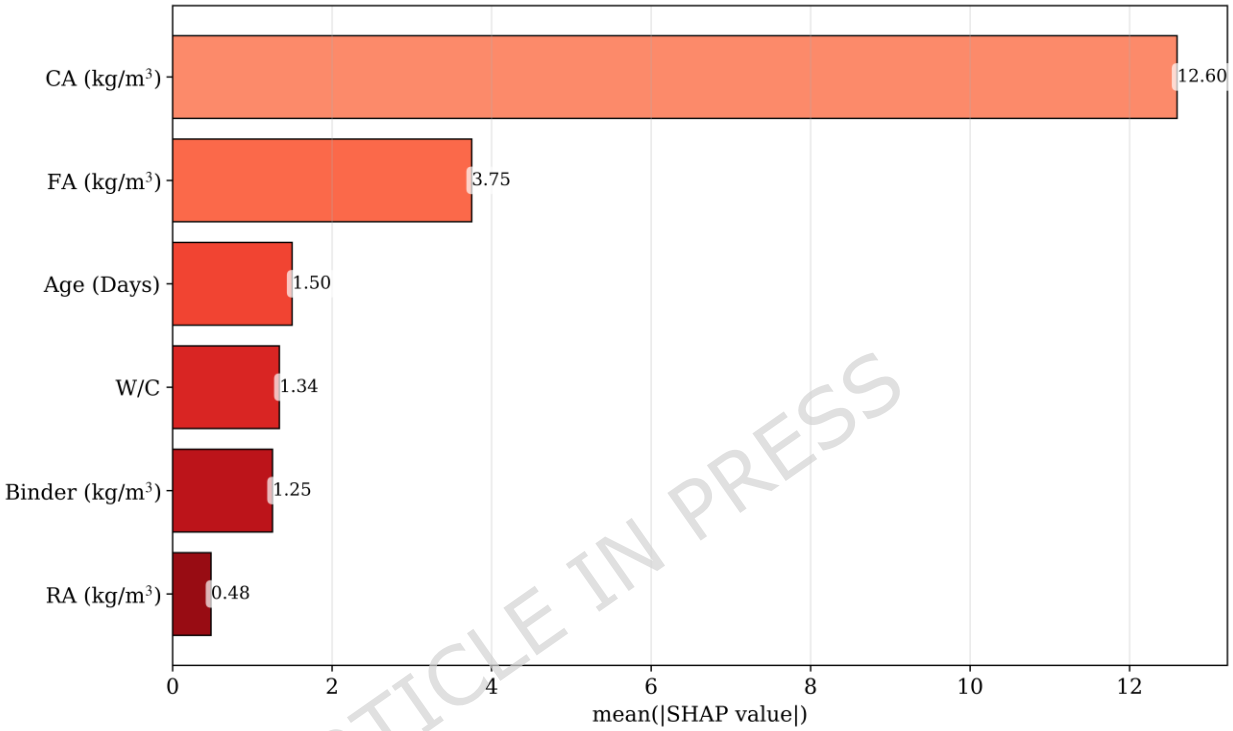


Figure 11: Effects of SHAP impact metrics on the model outcomes for predicting compressive strength.

Figure 11 illustrates the SHAP summary plot, which shows how each input feature affects the predicted compressive strength of all the concrete block samples. The horizontal line of each point indicates the SHAP value, which shows how much that feature changes the predicted strength relative to the baseline. Points on the right correspond to positive SHAP values, suggesting that specific feature values push the prediction towards higher compressive strength, whereas points on the left correspond to negative SHAP values, indicating a reduction in strength. The vertical ordering of features reflects their overall importance, with the most influential variables positioned at the top. The color gradient encodes the actual feature value for each instance, enabling simultaneous visualization of both directions of effect. Higher CA contents significantly increase predicted strength in this SHAP summary plot, while lower CA slightly decreases it. This is undoubtedly the most significant feature. At higher values, the effect of FA is weaker and generally

ARTICLE IN PRESS

positive. Strength can usually be improved by longer curing ages, although this effect is only moderate. Strength with negative SHAP values tends to decrease with a higher W/C, while it gradually rises with a lower W/C. Although it has a smaller effect than CA, a higher binder content certainly improves strength. Subsequently, in this dataset, predicted strength typically increases according to elevated RA content. Furthermore, this helps confirm that the learned relationships align with accepted concrete technology principles, such as the beneficial effects of proper binder and curing and the detrimental effects of excessive water content on compressive strength.



ARTICLE IN PRESS

Figure 12. Average absolute SHAP value of the significance of the compressive strength prediction

Figure 12 displays a bar chart of the mean absolute SHAP values for all input variables. This shows how important they are for predicting the compressive strength of concrete blocks made with waste aggregates. This shows how strongly that feature affects the model output. Features with larger bars have a greater impact on the predicted strength, while features with shorter bars have an inferior effect. The mean SHAP value for CA is by far the most extreme, so fluctuations in CA levels substantially affect the model's strength predictions. FA is the second-most important factor, indicating that the amount of FA used also significantly affects predicted strength. The age of the curing has a moderate effect, which means that strength gain over time is essential, but not as significant as the contents of the aggregate. Changes in W/C and binder content have similar effects, so changes in these parameters result in noticeable but minor variations in predictions. RA is the least important, which means that within the investigated ranges, its alterations have less of a consequence on compressive strength than the other mix components. In summary, the plot can

ARTICLE IN PRESS

be used to assess how well a model is understood. If a less relevant feature is overly dominant, it could indicate issues with the data or the model.

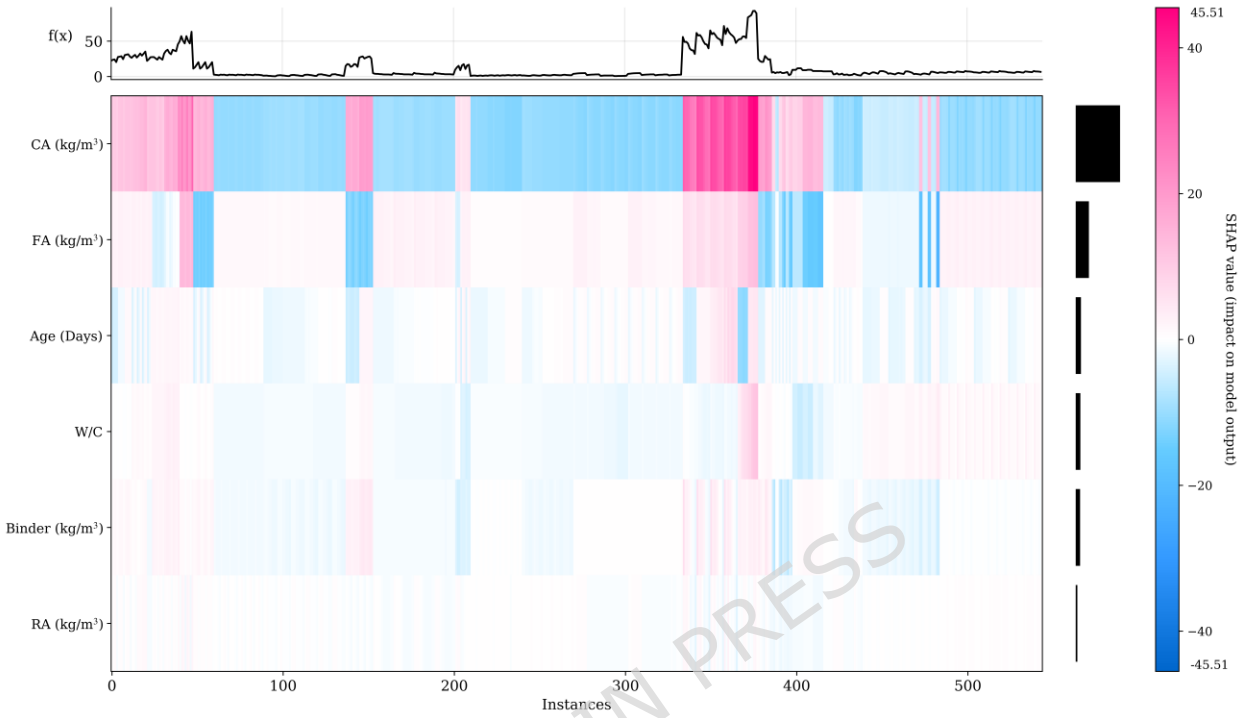


Figure 13: SHAP heat mapping for all data points.

Figure 13 shows a SHAP interaction plot examining how a selected feature affects the predicted compressive strength and how this effect might change when another variable interacts with it. The raw value of the main feature is shown on the horizontal axis, and the SHAP value, which indicates how much the feature contributed to the model's prediction for each sample, is shown on the vertical axis. Points higher up on the plot indicate that the specific feature value increases compressive strength, while points lower down indicate that the predicted strength decreases. This SHAP heatmap shows that CA has the strongest and most variable effect. Dark pink bands show cases where high CA sharply increases predicted strength, while blue bands show mixes where CA strongly lowers it. FA has a moderate, mostly positive effect, but there are some blue areas where certain FA levels reduce strength. In many cases, curing age makes things slightly stronger (to a pale pink), but the effect is usually weak. The W/C and binder content appear only in light shades, indicating they contribute little and are mostly local. RA doesn't change color much, which means it has minimal effect on the model's output.

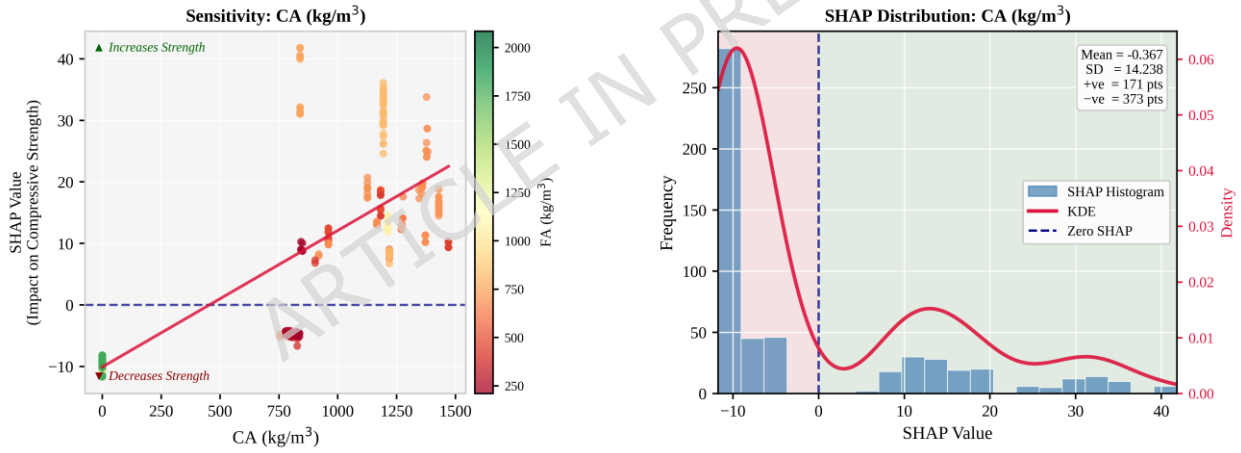
3.7. SHAP sensitivity analysis of input parameters

Figure 14 presents the SHAP sensitivity analysis for each of the six input parameters, where the left panels display SHAP values plotted against the raw feature values with a fitted regression

ARTICLE IN PRESS

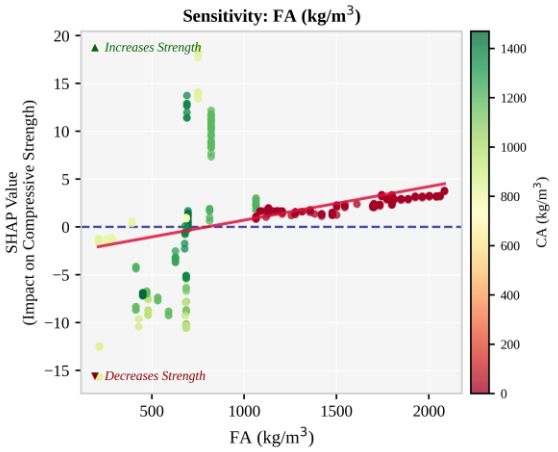
trend, while the right panels show the corresponding SHAP value distributions as histograms with overlaid KDE curves. CA (Fig. 14-a) shows the strongest positive sensitivity, with SHAP values rising from –10 at zero CA to over +40 at high CA, and exhibits the highest standard deviation (14.238), confirming its dominant role. FA (Fig. 14-b) presents an overall positive trend with the highest positive count (416 vs. 128) and a positive mean SHAP of +1.171, though outliers extend to about -12 at intermediate FA values. Curing age (Fig. 14-c) displays a monotonic positive trend, increasing from –2 at 1 day to nearly +7 at 91 days (306 positive vs. 238 negative). The W/C ratio (Fig. 14-d) exhibits a clearly negative sensitivity, with a downward trend line and a mean SHAP of –0.571 (368 negative vs. 176 positive points), confirming that higher W/C ratios reduce predicted strength. Binder content (Fig. 14-e) shows a positive trend, with SHAP values rising from about –2 at low binder levels to +1.5 at higher binder contents, although the mean is slightly negative (–0.312) due to the prevalence of low-binder samples. RA (Fig. 14-f) shows a negative trend line falling from about +0.2 at RA = 0 kg/m³ to –1.1 at RA = 400 kg/m³, yet its mean SHAP remains near zero (–0.036, SD = 0.636) with 299 positives vs. 245 negative points, indicating a comparatively weak overall influence. Collectively, these sensitivity patterns align with established principles of concrete science.

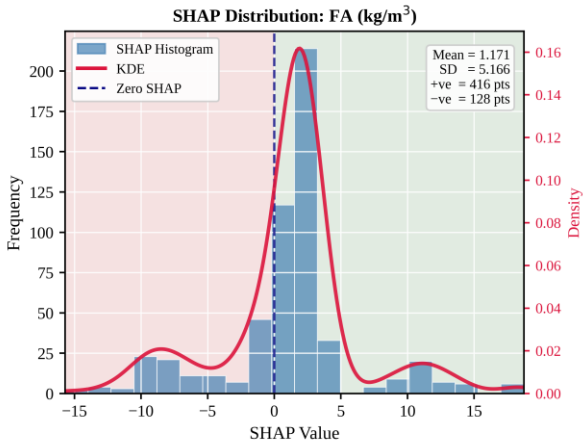
(a)



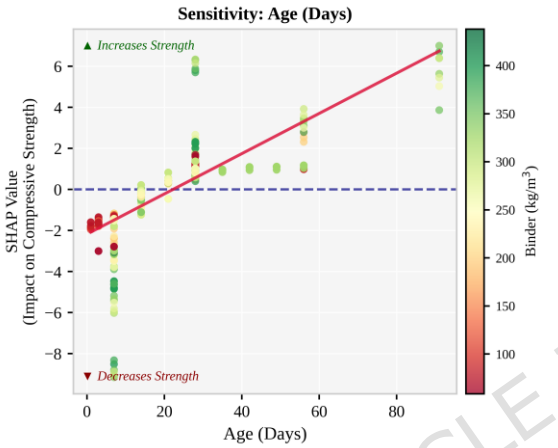
(b)

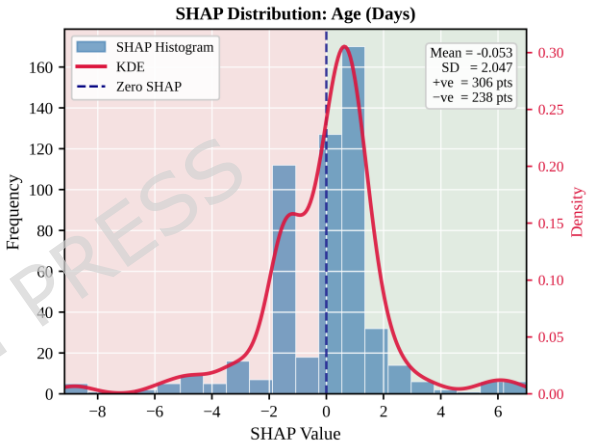
ARTICLE IN PRESS



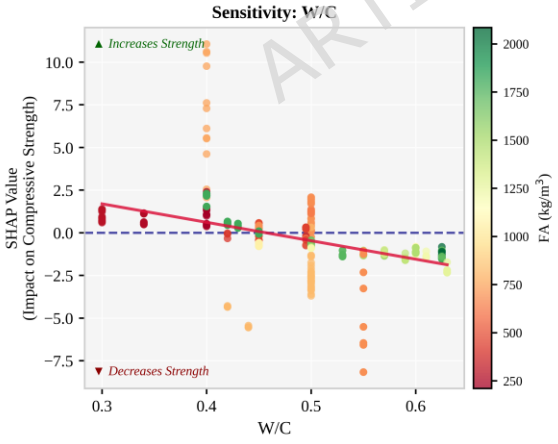


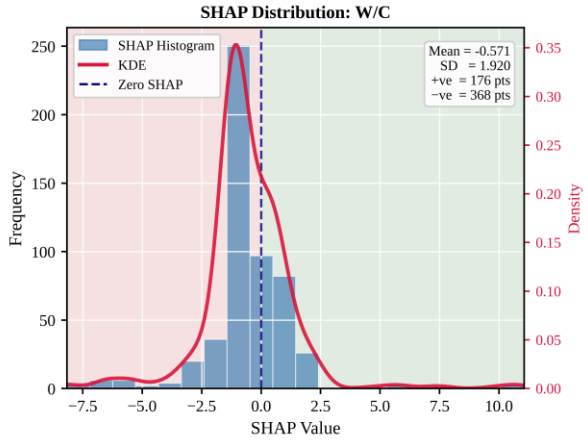
(c)





(d)





(e)

ARTICLE IN PRESS

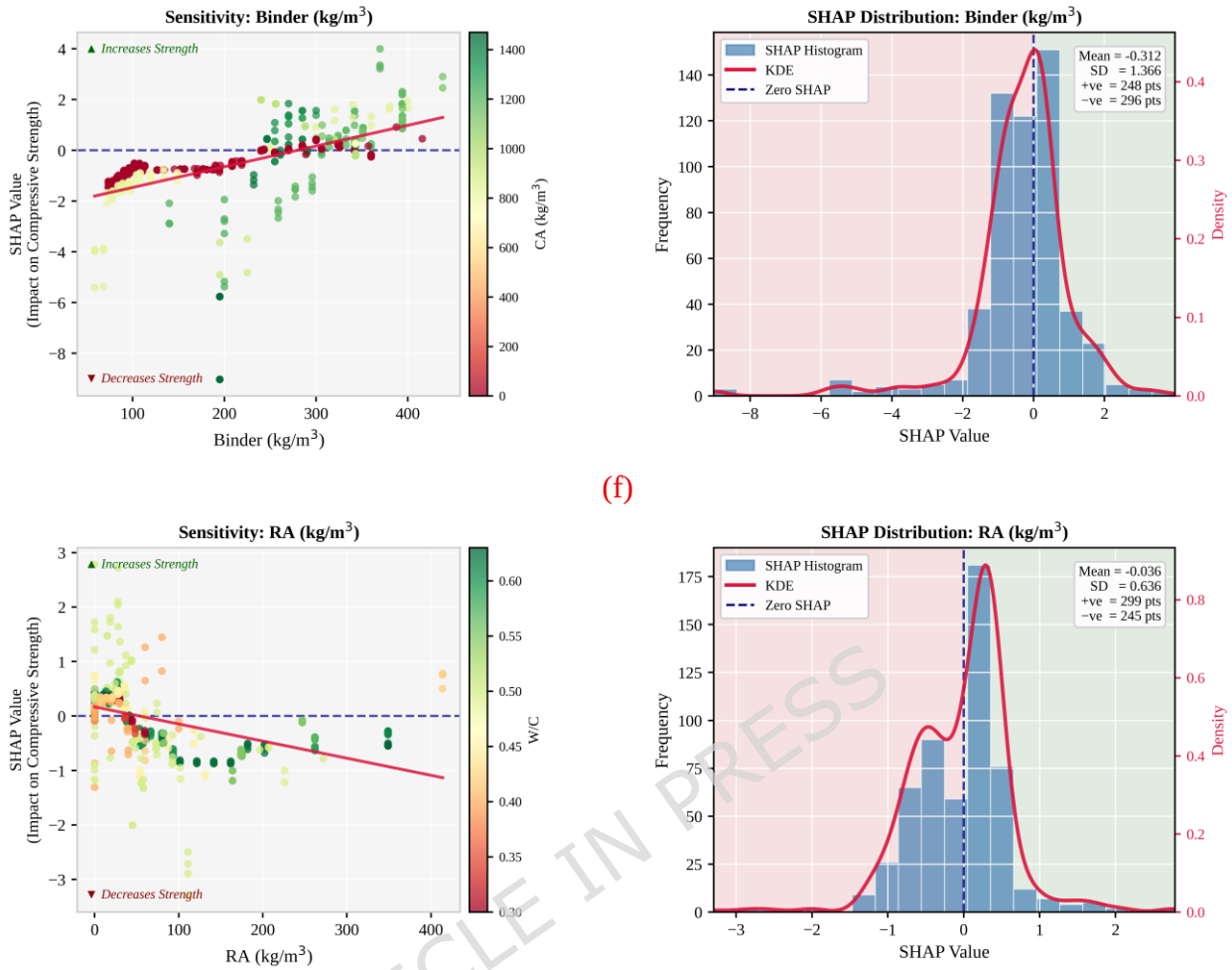


Figure 14. SHAP sensitivity analysis of input parameters for compressive strength prediction for the HBS (Top Model)

3.8. Uncertainty Analysis Test

In **Figure 15**, an uncertainty analysis test was conducted using both the training and testing datasets. It presents the comparative uncertainty values of the classification system across six feature groups: HSE, HRL, HWE, HML, HBS, and HFF. What stands out is a clear pattern-the testing uncertainty (those purple bars) is quite a bit higher than the training ones (gray bars) for every group. This type of difference is expected, as testing data typically introduces unseen variations that help reveal the model's true generalization capability. Models like HSE and HML exhibit moderate uncertainty during testing, suggesting they're holding up well with unfamiliar data. On the other hand, HRL has the highest testing uncertainty in the bunch, meaning it might add more unpredictability to the model's predictions than the others. Meanwhile, HWE, HBS, and HFF keep things tighter, with lower overall uncertainty, indicating greater reliability and less

ARTICLE IN PRESS

variability in results, whether in training or testing. Overall, this analysis gives us confidence that the model is pretty stable; training uncertainties stay low and under control across the board.

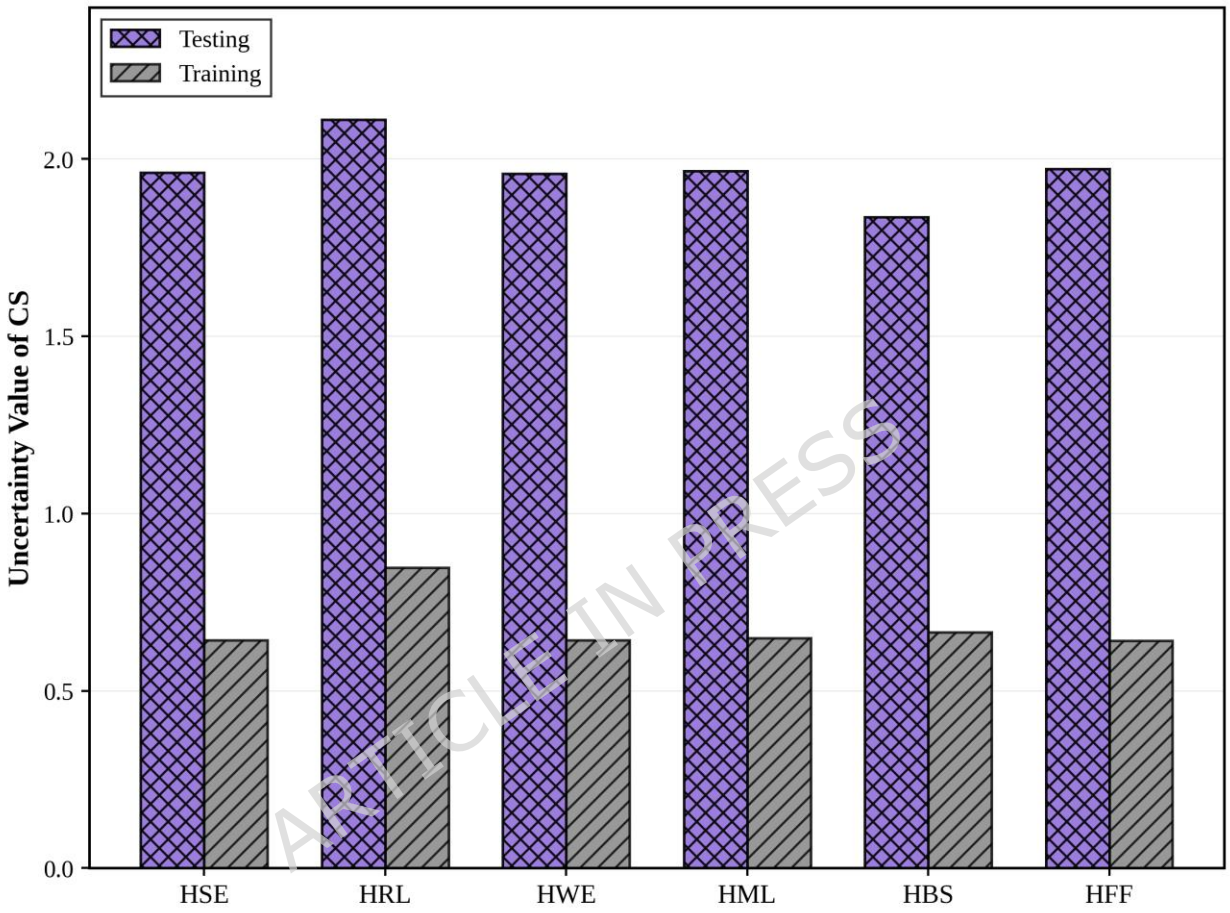


Figure 15: The uncertainty analysis test of evaluation results for compressive strength

3.9. Individual Conditional Expectation (ICE) plot analysis

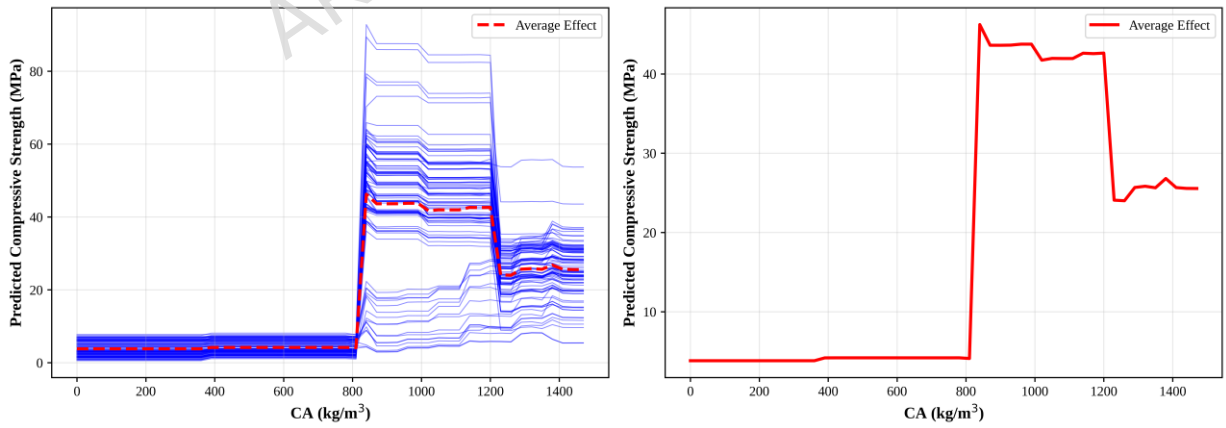
Heterogeneous feature effects on predicted compressive strength were visualized using ICE analysis, in which each blue curve shows the prediction trajectory of a single sample as a single feature is varied while all other features are held constant. The average effect (partial dependence) across all samples is shown by the red line, which demonstrates the various ways in which material parameters affect concrete strength. The content of FA varied greatly among samples and showed complex, non-monotonic behavior (**Figure 16-a, b**). Three distinct zones were identified: predictions remained stable with little variation (5-15 MPa) at low FA content (150-700 kg/m³); individual curves in a transition zone (700-900 kg/m³) showed dramatic divergence, with some

ARTICLE IN PRESS

samples reaching 90 MPa and others declining; and curves converged toward varied but stable strength levels beyond 900 kg/m³. Initial stability at 9.5 MPa, a spike to 15.5 MPa at about 750 kg/m^3, a decline to 14 MPa at moderate levels, and a recovery to 15.5 MPa at maximum FA content were the characteristic patterns of the average effect. This variability shows that the effects of FA are highly context-dependent, varying with mixture proportions, and illustrates its various functions in microstructure development, workability control, and void filling.

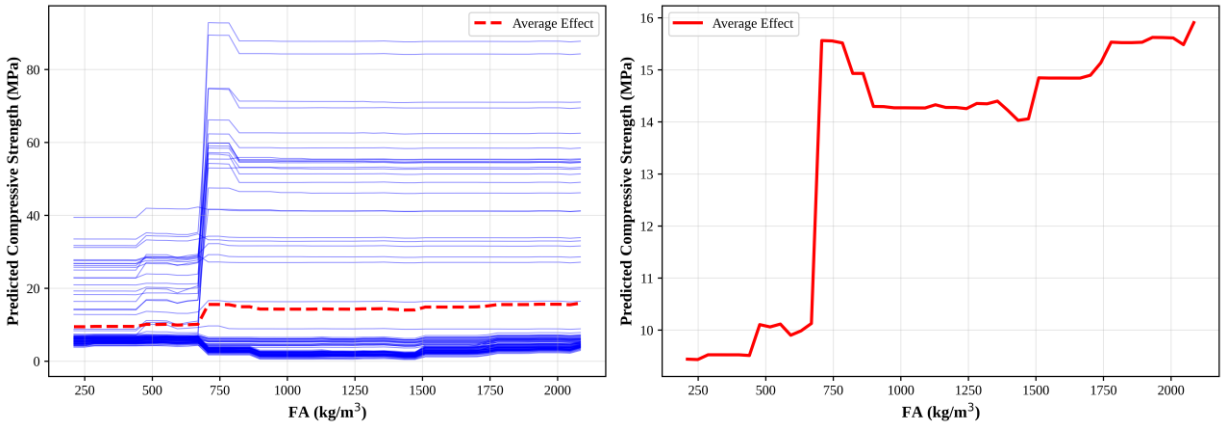
The most striking threshold behavior was shown by CA content (**Figure 16-c, d**). All samples showed consistently low strength (2-7 MPa) with horizontal ICE curves below 700 kg/m³. Nearly vertical transitions took place at 700-1000 kg/m³ as samples split into different strength classes (5-90 MPa). A systematic decrease in strength was noted above 1000 kg/m³. The average effect exhibited distinct inverted-U behavior, with minimal strength below 700 kg/m³, a peak at 46 MPa (900-1000 kg/m³), and a decline to 25 MPa at the maximum CA content. This threshold, which reflects aggregate skeleton formation through percolation mechanisms, signifies the crucial change from paste-dominated to aggregate-dominated composite behavior. The ICE curves for curing age showed monotonic, nearly parallel patterns (Figure 13-e, f), suggesting that the hydration kinetics were the same for all mixture designs. The average effect increased from 9.5 MPa (1 day) to 14.5 MPa (91 days), with rapid strength gain during the first 7-8 days, moderate increases through 28 days, and minimal development thereafter. The significant differences between the parallel curves for age and the ICE curves for FA and CA highlight important interaction effects, indicating that a comprehensive mixture design is necessary to achieve the desired performance.

ARTICLE IN PRESS

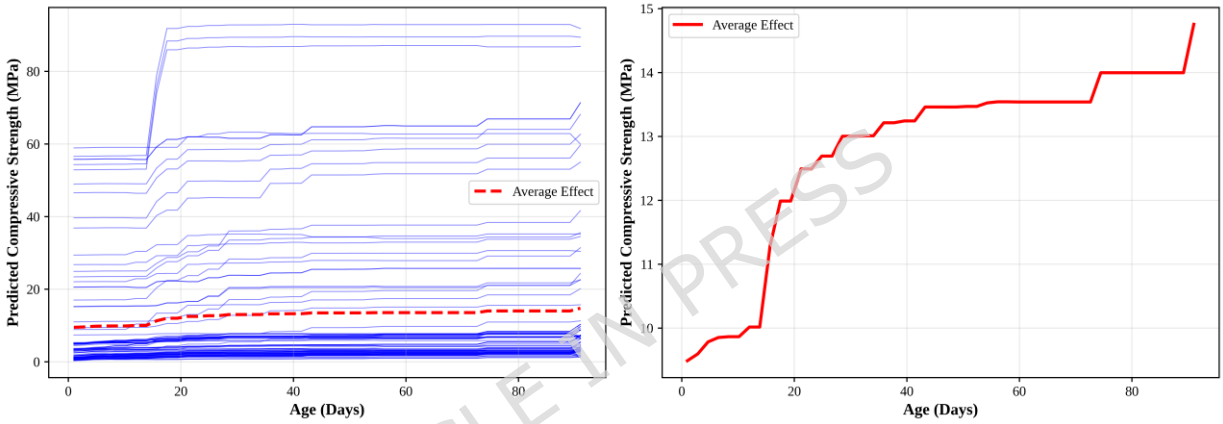


(a) Coarse Aggregate (kg/m^3) (b) Average Effect of CA (kg/m^3)

ARTICLE IN PRESS



(c) Fine Aggregate (kg/m^3) (d) Average Effect of FA (kg/m^3)



(e) Curing Age (Days) (f) Average Effect of Curing Age (Days)

Figure 16: ICE analysis results for the top three input features

3.10. Graphical User Interface (GUI)

A simple, user-friendly Graphical User Interface (GUI) in **Figure 17** was developed to enable quick prediction of the compressive strength of hollow concrete blocks using the trained hybrid machine learning model. The GUI contains 6 input fields for the key parameters-RA, W/C, binder content, FA, CA, and curing age- each parameter is entered manually by the user. After entering the values, the user clicks the “Predict” button, and the estimated compressive strength (in MPa) is displayed in a highlighted output box. A “Clear” button is also added to reset all input fields and the result. This interface provides a user-friendly and practical way to apply the model for mix design evaluation and rapid concrete strength estimation.

ARTICLE IN PRESS

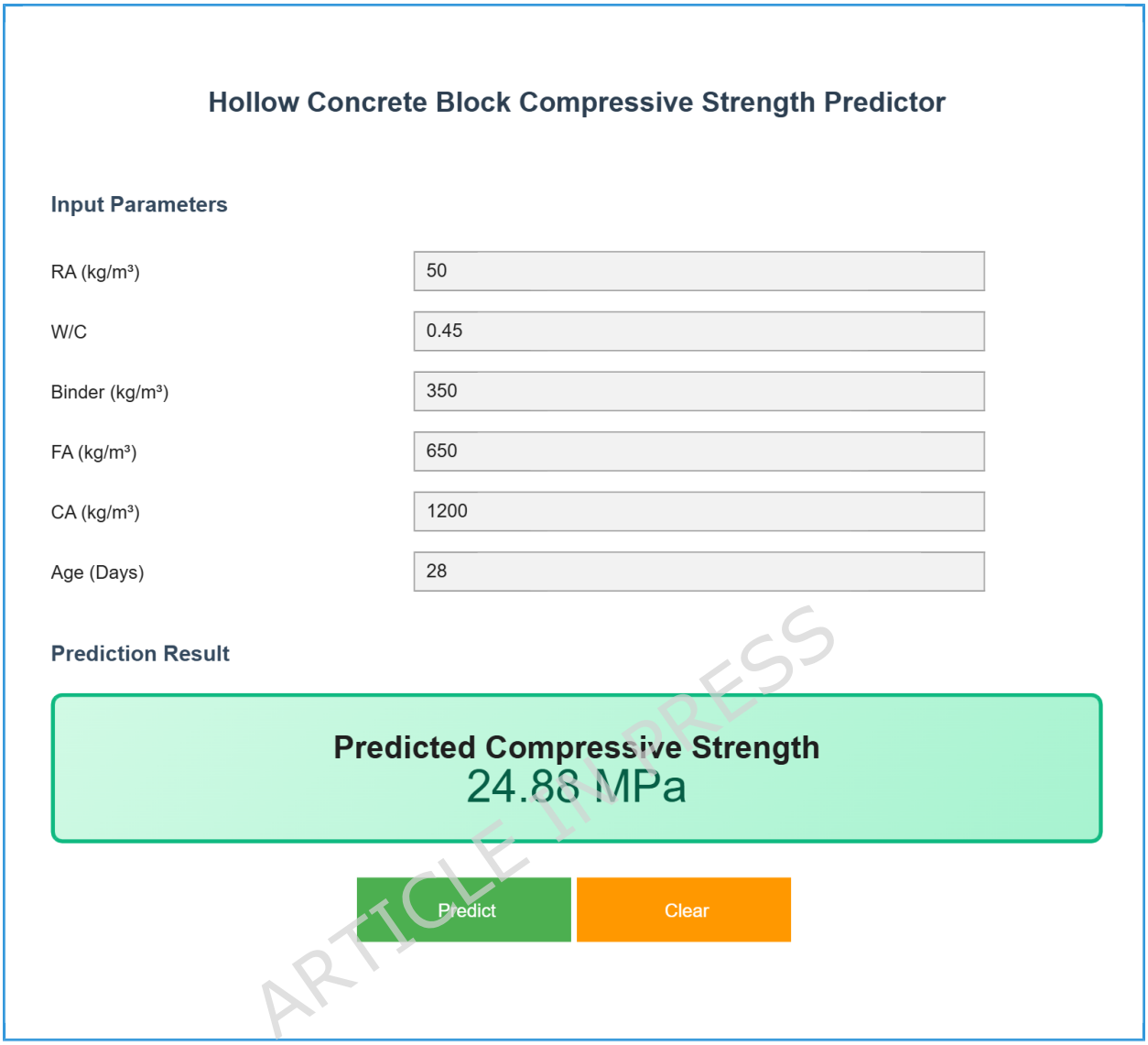


Figure 17: Graphical User Interface of the developed software.

4. Comparison with previous research

The study by Singh et al. [85] utilized various regression algorithms, including multiple linear regression, K-nearest neighbors, support vector regression, decision trees, random forests, extra trees, and gradient boosting, to analyze the impact of waste marble powder on concrete using a dataset of 720 samples. This effectiveness was evaluated using various statistical metrics, and experiments show that the random forest model is the best at predicting compressive strength, with an R^2 of 0.926 and a mean absolute error of 1.608. Salimbahrami et al. [86] have proposed recycling concrete waste and using it to make green concrete again. The results of 124 test specimens are more in agreement with the SVM results, and both artificial intelligence techniques, ANN and SVM, showed fairly equal coefficients of consistency. Chakravarthy HG et al. [101]

ARTICLE IN PRESS

explore the use of machine-learning techniques to model the compressive strength of Self-Compacting Concrete mixes, using 384 data points. With a comparatively low mean absolute error (0.52 MPa) during the testing phase, the CBR model outperformed the other ML models.The artificial neural network (ANN), boosting, and AdaBoost machine learning (ML) techniques were used in the study by Ahmad et al. to forecast the compressive strength of high-calcium fly ash-based geopolymer concrete [87]. A comparison of the two methods found that the ensemble ML approaches, AdaBoost and boosting, outperformed the individual ML technique (ANN) in terms of prediction performance. A comprehensive dataset comprising 400 mixtures was extracted and examined by Faraj et al., and four different approaches were proposed to forecast the compressive strength of self-compacting concrete mixes made with recycled plastic aggregates[88] with an R^2 value of 0.973, the ANN model performed better at predicting compressive strength.

Table 6: Compressive strength prediction details in the previous research.

ARTICLE IN PRESS

ARTICLE IN PRESS

SI No.	Input Features	Replaced Aggregate	No. of Data	ML Algorithms Used	Best ML Model	Predicted Feature	Evaluation Parameter		Reference
							R^2 Value	RMSE Value	
1.	Recycled aggregate (RA), water-to-cement ratio (W/C), binder content, fine aggregate (FA), coarse aggregate (CA), and curing time	Waste-aggregates	544	HSE, HRL, HWE, HML, HBS, and HFF	HBS	Compressive strength of waste-aggregate concrete blocks	0.987	1.836	Present Study
2.	Cement, Marble dust, Water, Superplasticizer, Slump, Aggregate, Sand	Waste Marble Powder (WMP)	720	MLR, KNN, SVR, DT, RF, ET, and GB	RF	Compressive strength of WMP-incorporated concrete	0.926	0.9259	Singh et al. 2023 [85]
3.	Coarse and fine aggregate, recycled aggregate, cement, water, and admixture	Recycled aggregate	124	ANN, SVM	SVM	Compressive strength of recycled aggregate concrete	0.974	-	Salimbahrami et al. 2021[86]
4.	SCC ingredients LECA, GGBS, IBMWA, density of SCC, water-to-binder (W/B) ratio, and superplasticizer (SP),	Incinerated Bio-Medical Waste Ash (IBMWA)	384	ANN, GTB, CBR	CBR	Compressive Strength of Waste-Aggregate Concrete	0.97	0.7395	Chakravarthy HG et al. 2023 [89]
5.	Recycled concrete aggregate content (RCA), and the age of concrete	Pavement demolition recycled aggregate	123	MLR	MLR	Compressive strength of recycled aggregate concrete	0.79	-	Sabău et al. 2022 [90]
6.	Amount of Na_2SiO_3, NaOH, SiO_2, Na_2O, the	Geopolymer	154	ANN, boosting,	Boosting	Compressive strength of	0.96	-	Ahmad et al. 2021 [87]

ARTICLE IN PRESS

ARTICLE IN PRESS

	molarity of NaOH, and the age of the curing			and AdaBoost		geopolymer concrete			
7.	Cement, blast furnace slag, fly ash, water, superplasticizer, coarse aggregate, fine aggregate, and curing age	Recycled aggregate	1030	ANN	ANN	Compressive strength of recycled aggregate concrete	0.946	-	Mohamad Ali Ridho et al. 2021 [91]
8.	RP aggregates by weight, binder, w/b ratio, SP content, natural fine aggregate content, natural coarse aggregate content, curing time by days	Recycled plastic aggregates and industrial waste ashes	400	ANN, nonlinear model, linear relationship model, and multi-logistic model	ANN	Compressive strength of self-compacting concrete incorporating recycled plastic aggregates and industrial waste ashes	0.973	5.46	Faraj et al. 2022 [88]

ARTICLE IN PRESS

5. Conclusion

This study successfully developed and evaluated six novel hybrid machine learning frameworks for predicting the compressive strength of concrete blocks (HCB) incorporating waste aggregates. A total of six key input parameters were evaluated, with 544 data samples for compressive strength prediction, all sourced from previous studies. Hyperparameter optimization and rigorous cross-validation were conducted to ensure robust model performance. Eighty per cent of these resources were meant for training, whereas twenty per cent were meant for testing. Using advanced ensemble models, including Hybrid Stacked Ensemble (HSE), Hybrid Residual Learning (HRL), Hybrid Weighted Ensemble (HWE), Hybrid Meta-Learning (HML), Hybrid Bayesian Stacking (HBS), and Hybrid Feature Fusion (HFF). Each hybrid model combined multiple base learners (Random Forest, XGBoost, Artificial Neural Networks) with sophisticated meta-learning approaches. Among the models, the novel Hybrid Bayesian Stacking (HBS) and Hybrid Stacked Ensemble (HSE) achieved superior performance, demonstrating excellent generalization between training and testing phases, with R^2 values exceeding 0.985.

Furthermore, Shapley Additive Explanations (SHAP), ICE Plots, and a Graphical User Interface (GUI) were used to analyze the contributions and interactions of input materials to the prediction of compressive strength. Lastly, nine evaluation criteria were used to check how well the models worked and how accurate they were. Based on these results, subsequent findings can be derived from the current study.

ARTICLE IN PRESS

- From the comprehensive analysis, it is observed that concrete block compressive strength is significantly influenced by multiple variables, with CA (0.66) and binder content (0.39) demonstrating the strongest positive correlation. Conversely, FA and W/C have negative impacts, particularly in high-strength regions, while curing age predominantly contributes positively to sustainable concrete production when properly proportioned in mixture designs.
- The comparative analysis reveals that novel Hybrid Bayesian Stacking (HBS) is the best approach for predicting concrete block compressive strength. It achieves exceptional performance with $R^2 = 0.9987$, demonstrating superior capability in capturing complex nonlinear relationships. Secondly, the Hybrid Stacked Ensemble (HSE) also delivers excellent results, with $R^2 = 0.9864$, RMSE = 1.92 MPa, and MAE = 0.91 MPa, establishing it as a highly balanced and robust method that effectively combines multiple base learners via Ridge regression meta-learning.
- The performance metrics across all hybrid models indicate exceptional predictive capability, with R^2 values ranging from 0.9756 to 0.9987, RMSE values between 1.92 and 3.85 MPa. These results significantly outperform conventional empirical equations and demonstrate the practical viability of machine-learning-based approaches for quality control, mix-design optimization, and rapid strength assessment in concrete block manufacturing facilities.
- Benchmarked against seven prior studies on waste-aggregate concrete, the developed hybrid models outperform all previously reported results, with HBS (test $R^2 = 0.987$) surpassing Random Forest ($R^2 = 0.926$), SVM ($R^2 = 0.974$), and ANN-based approaches ($R^2 = 0.973$), confirming the superiority of the proposed hybrid framework.
- According to the SHAP and ICE analysis, amounts of Fine Aggregate (kg/m^3) and Coarse Aggregate (kg/m^3) are the most impactful parameters in governing compressive capacity. Again, curing age exhibited the highest feature importance, demonstrating strong positive contributions to strength development, particularly after 28 days of hydration. Binder content and aggregate proportions revealed nuanced interaction effects, with optimal combinations yielding maximum compressive strength.
- To further integrate these advanced prediction models into a practical engineering tool, a graphical user interface (GUI) was developed, allowing designers to estimate compressive strength openly, honestly, and accurately.

The successful integration of novel hybrid machine learning architectures with comprehensive interpretability analysis addresses a critical gap in traditional black-box prediction methods. The SHAP-based feature importance analysis not only validates model predictions against established concrete technology principles but also provides transparent decision-making support essential for regulatory compliance and engineering practice.

ARTICLE IN PRESS

5.1. Limitations and Future Studies

The methodologies, tools, and insights presented in this study provide a robust framework for future research in computational materials science and offer practical instruments to accelerate the development and adoption of eco-friendly concrete technologies in the global construction industry, ultimately reducing environmental impact and enhancing resource efficiency in the built environment.

Moreover, this study achieved exceptional predictive accuracy and model interpretability, and several promising avenues for future research emerge. Expanding the dataset to include additional geographic regions, diverse waste-material sources, and varied environmental curing conditions would further enhance the model's generalizability across global construction contexts. Integration of additional input features, such as aggregate particle morphology, chemical composition parameters, mineralogical characteristics, and microstructural properties, could provide even deeper insights into the mechanisms of strength development. Investigation of hybrid models to predict other critical concrete properties beyond compressive strength, including tensile and flexural strengths, durability indicators such as permeability and chloride resistance, and long-term performance metrics, would extend the utility of these methodologies. The GUI tool has not undergone formal user acceptance testing or integration with structural design workflows, limiting its utility to illustrative demonstrations. Development of multi-objective optimisation frameworks that simultaneously consider strength, cost, and environmental impact could provide holistic solutions for sustainable concrete design.

ARTICLE IN PRESS

ARTICLE IN PRESS

Appendix 1: Supplementary materials

Reference	No. of Test	Temperature (°C)	W/C	FA (kg/m³)	Binder (kg/m³)	RA (kg/m³)	CA (kg/m³)	Compressive Strength (MPa)
T. Dela Cruz et al.2020 [92]	24	0.55	343	686	0 - 247	754.60 - 1372	14 - 28	6.24 - 13.69
J S Lumbab et al.2023 [93]	12	0.50	170.27 - 243.24	1702.70	0 - 72.97	0	7 - 28	1.50 - 4.80
M. Ibrahim 2024 [94]	48	0.60	73.54 - 113.14	1131.43	0 - 93.25	0	1 - 28	0.31 - 3.65
D. Lasco et al. 2017 [95]	5	0.50	288.80 - 415.80	1118.40 - 1610.60	0 - 272	0	0 - 28	1.05 - 3.58
E. Ephraim et al. 2012 [96]	12	0.45	240 - 320	480	0 - 38.70	960	7 - 28	10 - 22
M. Al-Tarbi et al. 2022 [97]	12	0.495	195 - 250	393 - 681	0 - 226	828 - 1470	7 - 28	1.87 - 6.55
F.A. Olutoge 2009[98]	29	0.60	126.57 - 219.44	1084.97 - 1316.65	0 - 57.74	0	28	1.70 - 2.78
Joyklad et al. 2025 [99]	64	0.53 - 0.63	326	1206 - 1745	0 - 349	0	7 - 56	0.50 - 4.80
Mitikie et al. 2025 [100]	12	0.45	306 - 360	1064	0 - 54	1212	7 - 28	20.01 - 32.12
Massoud et al. 2018 [101]	9	0.42 - 0.44	140 - 200	414 - 813	0 - 414	1219	7 - 56	8.93 - 16.68
Yayena et al. 2024 [102]	60	0.40 - 0.45	240 - 300	1800	0 - 28	0	7 - 28	4.10 - 9.40
S. Khandagale et al. 2023 [103]	12	0.50	232 - 290	696	0 - 58	1429	7 - 28	19.76 - 35.7
Saravanan et al. 2016[104]	8	0.45	306.6 - 438	686.24	0 - 131.40	1126	7 - 28	20 - 29
Omran et al. 2025 [105]	24	0.50	255 - 300	628 - 690	0 - 45	1270 - 1382	28	22.56 - 63.74
Khamput et al. 2024[106]	48	0.625	208.50	1696.50 - 2084.50	0 - 202.10	0	7 - 28	2.50 - 5.50
Zareei et al. 2017[107]	12	0.40	300 - 400	750	0 - 100	840	7 - 28	50.84 - 93.28
A. A. Raheem 2013 [108]	30	0.6	83.10 - 110.80	1476.90	0 - 27.70	0	7 - 56	0.75 - 2.80
Kamau et al. 2018[109]	32	0.5	258.75 - 369.65	821.28	0 - 110.90	1193.50	7 - 91	31.20 - 71.30
Sojobi et al. 2021 [110]	30	0.45	306 - 360	1064	0 - 54	0	7 - 28	0.83 - 2.21
Subba et al. 2023 [111]	16	0.45	394	413.70 - 591	0 - 177.30	1182	7 - 28	13.48 - 31.42
Mitikie et al. 2022[112]	45	0.3 - 0.4	58.60 - 148.79	210.13 - 287.35	0 - 59.56	777.97 - 850.10	3 - 28	2.50 - 8.50

ARTICLE IN PRESS

Credit authorship contribution statement

Md Arifuzzaman: Supervision, Writing – review & editing, Funding acquisition. **S.M. Shishir Ahmed:** Writing-original draft, Software, Exploratory Data Analysis and visualization, Methodology, Data curation, Investigation. **Md. Abdul Khaled:** Writing – original draft, literature review, Data visualization, and Investigation. **Md. Sameen Yasar Siddiq:** Data Collection & Editing. **Prajnat Barua:** Writing – Introduction, Literature Data Collection & Analysis, Referencing. **Md. Mahamudul Hasan:** Writing - Data curation, Data Visualization, Investigation. **Sourov Paul:** Writing-original draft, Writing - review & editing, Validation, Supervision.

Data availability statement

The datasets utilized during the current study are available on GitHub. (https://github.com/Shishirahmed153907/Hollow-Concrete-Block-Dataset)

Funding Statement: This work was supported by the Deanship of Scientific Research, Vice Presidency for Graduate Studies and Scientific Research, King Faisal University, Saudi Arabia [Grant No. KFU261259]

Conflicts of Interest: The authors declare no conflicts of interest

ARTICLE IN PRESS

References:

1. Cheng, D.; Reiner, D.M.; Yang, F.; Cui, C.; Meng, J.; Shan, Y.; Liu, Y.; Tao, S.; Guan, D. Projecting Future Carbon Emissions from Cement Production in Developing Countries. *Nat. Commun.* **2023**, *14*, doi:10.1038/s41467-023-43660-x.

2. Andrew, R.M. Global CO 2 Emissions from Cement Production. *Earth Syst. Sci. Data* **2018**, *10*, 195–217.

ARTICLE IN PRESS

3. Environment, U.N.; Scrivener, K.L.; John, V.M.; Gartner, E.M. Eco-Efficient Cements: Potential Economically Viable Solutions for a Low-CO2 Cement-Based Materials Industry. *Cem. Concr. Res.* **2018**, *114*, 2–26.

4. Monteiro, P.J.M.; Miller, S.A.; Horvath, A. Towards Sustainable Concrete. *Nat. Mater.* **2017**, *16*, 698–699.

5. Olsson, J.A.; Miller, S.A.; Alexander, M.G. Near-Term Pathways for Decarbonizing Global Concrete Production. *Nat. Commun.* **2023**, *14*, doi:10.1038/s41467-023-40302-0.

6. Xiao, J.; Li, W.; Fan, Y.; Huang, X. An Overview of Study on Recycled Aggregate Concrete in China (1996–2011). *Constr. Build. Mater.* **2012**, *31*, 364–383.

7. Bergmans, J.; Kazemi Kamyab, H.; Ghosh, D.; Van Mierloo, P.; Carens, H.; Nielsen, P. Carbonation of Recycled Concrete Aggregates for New Concrete and Concrete Fines to Make Cement-Free Hollow Blocks. *Sustainability* **2024**, *16*, 3494.

8. Kou, S.; Poon, C.S. Enhancing the Durability Properties of Concrete Prepared with Coarse Recycled Aggregate. *Constr. Build. Mater.* **2012**, *35*, 69–76.

9. Habeeb, G.A.; Mahmud, H. Bin Study on Properties of Rice Husk Ash and Its Use as Cement Replacement Material. *Materials research* **2010**, *13*, 185–190.

10. Gastaldini, A.L.G.; Isaia, G.C.; Saciloto, A.P.; Missau, F.; Hoppe, T.F. Influence of Curing Time on the Chloride Penetration Resistance of Concrete Containing Rice Husk Ash: A Technical and Economical Feasibility Study. *Cem. Concr. Compos.* **2010**, *32*, 783–793.

11. Chao-Lung, H.; Le Anh-Tuan, B.; Chun-Tsun, C. Effect of Rice Husk Ash on the Strength and Durability Characteristics of Concrete. *Constr. Build. Mater.* **2011**, *25*, 3768–3772.

12. Rukzon, S.; Chindaprasirt, P. Utilization of Bagasse Ash in High-Strength Concrete. *Mater. Des.* **2012**, *34*, 45–50.

13. Ganesan, K.; Rajagopal, K.; Thangavel, K. Rice Husk Ash Blended Cement: Assessment of Optimal Level of Replacement for Strength and Permeability Properties of Concrete. *Constr. Build. Mater.* **2008**, *22*, 1675–1683.

14. Sadek, D.M.; El-Attar, M.M.; Ali, H.A. Reusing of Marble and Granite Powders in Self-Compacting Concrete for Sustainable Development. *J. Clean. Prod.* **2016**, *121*, 19–32.

15. Aprianti, E.; Shafigh, P.; Bahri, S.; Farahani, J.N. Supplementary Cementitious Materials Origin from Agricultural Wastes–A Review. *Constr. Build. Mater.* **2015**, *74*, 176–187.

16. Thomas, C.; Setién, J.; Polanco, Ja.; Alaejos, P.; De Juan, M.S. Durability of Recycled Aggregate Concrete. *Constr. Build. Mater.* **2013**, *40*, 1054–1065.

17. Rashad, A.M. A Comprehensive Overview about the Influence of Different Additives on the Properties of Alkali-Activated Slag–A Guide for Civil Engineer. *Constr. Build. Mater.* **2013**, *47*, 29–55.

ARTICLE IN PRESS

ARTICLE IN PRESS

18. Juenger, M.C.G.; Siddique, R. Recent Advances in Understanding the Role of Supplementary Cementitious Materials in Concrete. *Cem. Concr. Res.* **2015**, *78*, 71–80.

19. Lothenbach, B.; Scrivener, K.; Hooton, R.D. Supplementary Cementitious Materials. *Cem. Concr. Res.* **2011**, *41*, 1244–1256.

20. Sahmaran, M.; Yaman, I.O. Hybrid Fiber Reinforced Self-Compacting Concrete with a High-Volume Coarse Fly Ash. *Constr. Build. Mater.* **2007**, *21*, 150–156.

21. Yu, Y.; Zhou, L.; Khodadadi, N.; Nanni, A. Size Effects on Uniaxial Compression and Tension in Recycled Aggregate Concrete Fabricated Using Conventional and Equivalent Mortar Volume Techniques. *Journal of Materials in Civil Engineering* **2026**, *38*, doi:10.1061/JMCEE7.MTENG-20732.

22. Özbay, E.; Erdemir, M.; Durmuş, H.İ. Utilization and Efficiency of Ground Granulated Blast Furnace Slag on Concrete Properties–A Review. *Constr. Build. Mater.* **2016**, *105*, 423–434.

23. Zega, C.J.; Di Maio, Á.A. Use of Recycled Fine Aggregate in Concretes with Durable Requirements. *Waste management* **2011**, *31*, 2336–2340.

24. Lipton, Z.C. The Mythos of Model Interpretability: In Machine Learning, the Concept of Interpretability Is Both Important and Slippery. *Queue* **2018**, *16*, 31–57.

25. Rudin, C. Stop Explaining Black Box Machine Learning Models for High Stakes Decisions and Use Interpretable Models Instead. *Nat. Mach. Intell.* **2019**, *1*, 206–215.

26. Behnood, A.; Ziari, H. Effects of Silica Fume Addition and Water to Cement Ratio on the Properties of High-Strength Concrete after Exposure to High Temperatures. *Cem. Concr. Compos.* **2008**, *30*, 106–112.

27. Shehadeh, A.; Alshboul, O.; Saleh, E. Enhancing Safety and Reliability in Multistory Construction: A Multi-State System Assessment of Shoring/Reshoring Operations Using Interval-Valued Belief Functions. *Reliab. Eng. Syst. Saf.* **2024**, *252*, 110458, doi:10.1016/j.ress.2024.110458.

28. Alshboul, O.; Shehadeh, A.; Saleh, E. Advancing Construction Quality Management: An Integrated Evidential Reasoning and Belief Functions Framework. *J. Constr. Eng. Manag.* **2025**, *151*, doi:10.1061/JCEMD4.COENG-15969.

29. Chopra, P.; Sharma, R.K.; Kumar, M. Prediction of Compressive Strength of Concrete Using Artificial Neural Network and Genetic Programming. *Advances in materials science and engineering* **2016**, *2016*, 7648467.

30. Young, B.A.; Hall, A.; Pilon, L.; Gupta, P.; Sant, G. Can the Compressive Strength of Concrete Be Estimated from Knowledge of the Mixture Proportions?: New Insights from Statistical Analysis and Machine Learning Methods. *Cem. Concr. Res.* **2019**, *115*, 379–388.

ARTICLE IN PRESS

31. Chou, J.-S.; Tsai, C.-F.; Pham, A.-D.; Lu, Y.-H. Machine Learning in Concrete Strength Simulations: Multi-Nation Data Analytics. *Constr. Build. Mater.* **2014**, *73*, 771–780.

32. Sah, A.K.; Hong, Y.M. Performance Comparison of Machine Learning Models for Concrete Compressive Strength Prediction. Materials 2024, 17, 2075 2024.

33. Kumar, R.; Kumar, D.R.; Wipulanusat, W.; Thongchom, C.; Samui, P.; Rai, B. Estimation of the Compressive Strength of Ultrahigh Performance Concrete Using Machine Learning Models. *Intelligent Systems with Applications* **2025**, *25*, 200471.

34. Chandra, S.S.; Kumar, R.; Arjunasamy, A.; Galagali, S.; Tantri, A.; Naganna, S.R. Predicting the Compressive Strength of Polymer-Infused Bricks: A Machine Learning Approach with SHAP Interpretability. *Sci. Rep.* **2025**, *15*, 8090.

35. DeRousseau, M.A.; Kasprzyk, J.R.; Srubar Iii, W. V Computational Design Optimization of Concrete Mixtures: A Review. *Cem. Concr. Res.* **2018**, *109*, 42–53.

36. Dao, D. Van; Ly, H.-B.; Trinh, S.H.; Le, T.-T.; Pham, B.T. Artificial Intelligence Approaches for Prediction of Compressive Strength of Geopolymer Concrete. *Materials* **2019**, *12*, 983.

37. Dietterich, T.G. Ensemble Methods in Machine Learning. In Proceedings of the International workshop on multiple classifier systems; Springer, 2000; pp. 1–15.

38. Shehadeh, A.; Alshboul, O. Enhancing Occupational Safety in Construction: Predictive Analytics Using Advanced Ensemble Machine Learning Algorithms. *Eng. Appl. Artif. Intell.* **2025**, *159*, 111761, doi:10.1016/j.engappai.2025.111761.

39. Li, Q.; Song, Z. Prediction of Compressive Strength of Rice Husk Ash Concrete Based on Stacking Ensemble Learning Model. *J. Clean. Prod.* **2023**, *382*, 135279.

40. Das, P.; Kashem, A. Hybrid Machine Learning Approach to Prediction of the Compressive and Flexural Strengths of UHPC and Parametric Analysis with Shapley Additive Explanations. *Case Studies in Construction Materials* **2024**, *20*, e02723.

41. Zhao, Y.; Goulias, D.; Saremi, S. Enhancing Prediction Accuracy of Concrete Compressive Strength Using Stacking Ensemble Machine Learning. *Computers and Concrete* **2023**, *32*, 233–246.

42. Zhang, J.; Li, D.; Wang, Y. Toward Intelligent Construction: Prediction of Mechanical Properties of Manufactured-Sand Concrete Using Tree-Based Models. *J. Clean. Prod.* **2020**, *258*, 120665.

43. Yu, Y.; Su, J.; Wu, B. A Hybrid Bayesian Model Updating and Non-Dominated Sorting Genetic Algorithm Framework for Intelligent Mix Design of Steel Fiber Reinforced Concrete. *Eng. Appl. Artif. Intell.* **2025**, *161*, 112071, doi:10.1016/j.engappai.2025.112071.

ARTICLE IN PRESS

44. Ahmed, H.U.; Mohammed, A.A.; Mohammed, A.S. The Role of Nanomaterials in Geopolymer Concrete Composites: A State-of-the-Art Review. *Journal of Building Engineering* **2022**, *49*, 104062.

45. Mangalathu, S.; Hwang, S.-H.; Jeon, J.-S. Failure Mode and Effects Analysis of RC Members Based on Machine-Learning-Based SHapley Additive ExPlanations (SHAP) Approach. *Eng. Struct.* **2020**, *219*, 110927.

46. Feng, D.-C.; Liu, Z.-T.; Wang, X.-D.; Chen, Y.; Chang, J.-Q.; Wei, D.-F.; Jiang, Z.-M. Machine Learning-Based Compressive Strength Prediction for Concrete: An Adaptive Boosting Approach. *Constr. Build. Mater.* **2020**, *230*, 117000.

47. Najigivi, A.; Khaloo, A.; Iraji zad, A.; Abdul Rashid, S. An Artificial Neural Networks Model for Predicting Permeability Properties of Nano Silica–Rice Husk Ash Ternary Blended Concrete. *Int. J. Concr. Struct. Mater.* **2013**, *7*, 225–238.

48. Asteris, P.G.; Mokos, V.G. Concrete Compressive Strength Using Artificial Neural Networks. *Neural Comput. Appl.* **2020**, *32*, 11807–11826.

49. Ni, H.-G.; Wang, J.-Z. Prediction of Compressive Strength of Concrete by Neural Networks. *Cem. Concr. Res.* **2000**, *30*, 1245–1250.

50. Chen, T. XGBoost: A Scalable Tree Boosting System. *Cornell University* **2016**.

51. Feng, D.-C.; Wang, W.-J.; Mangalathu, S.; Hu, G.; Wu, T. Implementing Ensemble Learning Methods to Predict the Shear Strength of RC Deep Beams with/without Web Reinforcements. *Eng. Struct.* **2021**, *235*, 111979.

52. Ke, G.; Meng, Q.; Finley, T.; Wang, T.; Chen, W.; Ma, W.; Ye, Q.; Liu, T.-Y. Lightgbm: A Highly Efficient Gradient Boosting Decision Tree. *Adv. Neural Inf. Process. Syst.* **2017**, *30*.

53. Prokhorenkova, L.; Gusev, G.; Vorobev, A.; Dorogush, A.V.; Gulin, A. CatBoost: Unbiased Boosting with Categorical Features. *Adv. Neural Inf. Process. Syst.* **2018**, *31*.

54. Han, Q.; Gui, C.; Xu, J.; Lacidogna, G. A Generalized Method to Predict the Compressive Strength of High-Performance Concrete by Improved Random Forest Algorithm. *Constr. Build. Mater.* **2019**, *226*, 734–742.

55. Duan, J.; Asteris, P.G.; Nguyen, H.; Bui, X.-N.; Moayedi, H. A Novel Artificial Intelligence Technique to Predict Compressive Strength of Recycled Aggregate Concrete Using ICA-XGBoost Model. *Eng. Comput.* **2021**, *37*, 3329–3346.

56. Zhang, J.; Ma, G.; Huang, Y.; Aslani, F.; Nener, B. Modelling Uniaxial Compressive Strength of Lightweight Self-Compacting Concrete Using Random Forest Regression. *Constr. Build. Mater.* **2019**, *210*, 713–719.

57. Vapnik, V. *The Nature of Statistical Learning Theory*; Springer science & business media, 2013; ISBN 1475732643.

ARTICLE IN PRESS

ARTICLE IN PRESS

58. Cheng, M.-Y.; Firdausi, P.M.; Prayogo, D. High-Performance Concrete Compressive Strength Prediction Using Genetic Weighted Pyramid Operation Tree (GWPOT). *Eng. Appl. Artif. Intell.* **2014**, *29*, 104–113.

59. Nguyen, H.A.T.; Pham, D.H.; Ahn, Y. Effect of Data Augmentation Using Deep Learning on Predictive Models for Geopolymer Compressive Strength. *Applied Sciences* **2024**, *14*, 3601.

60. Frazier, P.I. A Tutorial on Bayesian Optimization. *arXiv preprint arXiv:1807.02811* **2018**.

61. Brochu, E.; Cora, V.M.; De Freitas, N. A Tutorial on Bayesian Optimization of Expensive Cost Functions, with Application to Active User Modeling and Hierarchical Reinforcement Learning. *arXiv preprint arXiv:1012.2599* **2010**.

62. Alshboul, O.; Al-Shboul, K.; Shehadeh, A.; Tatari, O. Advancing Equipment Management for Construction: Introducing a New Model for Cost, Time and Quality Optimization. *Construction Innovation* **2026**, *26*, 1191–1217, doi:10.1108/CI-04-2024-0129.

63. Nguyen, H.; Vu, T.; Vo, T.P.; Thai, H.-T. Efficient Machine Learning Models for Prediction of Concrete Strengths. *Constr. Build. Mater.* **2021**, *266*, 120950.

64. Song, H.; Ahmad, A.; Farooq, F.; Ostrowski, K.A.; Maślak, M.; Czarnecki, S.; Aslam, F. Predicting the Compressive Strength of Concrete with Fly Ash Admixture Using Machine Learning Algorithms. *Constr. Build. Mater.* **2021**, *308*, 125021.

65. Hospedales, T.; Antoniou, A.; Micaelli, P.; Storkey, A. Meta-Learning in Neural Networks: A Survey. *IEEE Trans. Pattern Anal. Mach. Intell.* **2021**, *44*, 5149–5169.

66. Vanschoren, J. Meta-Learning: A Survey. *arXiv preprint arXiv:1810.03548* **2018**.

67. Wakjira, T.G.; Ebead, U.; Alam, M.S. Machine Learning-Based Shear Capacity Prediction and Reliability Analysis of Shear-Critical RC Beams Strengthened with Inorganic Composites. *Case Studies in Construction Materials* **2022**, *16*, e01008.

68. He, K.; Zhang, X.; Ren, S.; Sun, J. Deep Residual Learning for Image Recognition. In Proceedings of the Proceedings of the IEEE conference on computer vision and pattern recognition; 2016; pp. 770–778.

69. Szegedy, C.; Ioffe, S.; Vanhoucke, V.; Alemi, A. Inception-v4, Inception-Resnet and the Impact of Residual Connections on Learning. In Proceedings of the Proceedings of the AAAI conference on artificial intelligence; 2017; Vol. 31.

70. Huang, G.; Liu, Z.; Van Der Maaten, L.; Weinberger, K.Q. Densely Connected Convolutional Networks. In Proceedings of the Proceedings of the IEEE conference on computer vision and pattern recognition; 2017; pp. 4700–4708.

71. Cheng, J.; Xie, C.; Bian, W.; Tao, D. Feature Fusion for 3D Hand Gesture Recognition by Learning a Shared Hidden Space. *Pattern Recognit. Lett.* **2012**, *33*, 476–484.

ARTICLE IN PRESS

ARTICLE IN PRESS

72. Khalil, E.; Dai, H.; Zhang, Y.; Dilkina, B.; Song, L. Learning Combinatorial Optimization Algorithms over Graphs. *Adv. Neural Inf. Process. Syst.* **2017**, *30*.

73. Bengio, Y.; Courville, A.; Vincent, P. Representation Learning: A Review and New Perspectives. *IEEE Trans. Pattern Anal. Mach. Intell.* **2013**, *35*, 1798–1828.

74. Farooq, F.; Nasir Amin, M.; Khan, K.; Rehan Sadiq, M.; Javed, M.F.; Aslam, F.; Alyousef, R. A Comparative Study of Random Forest and Genetic Engineering Programming for the Prediction of Compressive Strength of High Strength Concrete (HSC). *Applied Sciences* **2020**, *10*, 7330.

75. Nhat-Duc, H.; Quoc-Lam, N. Towards Sustainable Construction: Estimating Compressive Strength of Waste Foundry Sand-Blended Green Concrete Using a Hybrid Machine Learning Approach. *Discover Civil Engineering* **2025**, *2*, 42.

76. Kandiri, A.; Golafshani, E.M.; Behnood, A. Estimation of the Compressive Strength of Concretes Containing Ground Granulated Blast Furnace Slag Using Hybridized Multi-Objective ANN and Salp Swarm Algorithm. *Constr. Build. Mater.* **2020**, *248*, 118676.

77. Wang, J.; Deng, J.; Li, S.; Du, W.; Zhang, Z.; Liu, X. Explainable Machine Learning for Multicomponent Concrete: Predictive Modeling and Feature Interaction Insights. *Materials* **2025**, *18*, 4456.

78. Agarwal, A.; Xiao, M.; Barter, R.; Ronen, O.; Fan, B.; Yu, B. PCS-UQ: Uncertainty Quantification via the Predictability-Computability-Stability Framework. *arXiv preprint arXiv:2505.08784* **2025**.

79. Hodson, T.O. Root Mean Square Error (RMSE) or Mean Absolute Error (MAE): When to Use Them or Not. *Geoscientific Model Development Discussions* **2022**, *2022*, 1–10.

80. Steurer, M.; Hill, R.J.; Pfeifer, N. Metrics for Evaluating the Performance of Machine Learning Based Automated Valuation Models. *Journal of Property Research* **2021**, *38*, 99–129.

81. Esmaeili-Falak, M. Optimized Gradient Boosting Model for Estimating Unconfined Compressive Strength of Pozzolanic Geopolymer-Stabilized Granular Materials Using Pufferfish Algorithm. *Transportation Infrastructure Geotechnology* **2026**, *13*, 106.

82. Esmaeili-Falak, M.; Letafat, A. Prediction of Unconfined Compressive Strength in Pozzolanic Geopolymer-Stabilized Granular Materials Using Tree-Based Models. *Transportation Infrastructure Geotechnology* **2025**, *12*, 247.

83. Borchelooei, M.S.; Esmaeili-Falak, M. Predicting Water Absorption in Hardened Concrete Using Machine Learning: A Comparative Analysis of XGBoost Optimization Methods. *International Journal of Pavement Research and Technology* **2026**, 1–20.

84. Esmaeili-Falak, M.; Sojoudi, B. Enhancing Dimensional Stability in Cement Pastes: A Machine Learning Approach with Metaheuristic-Optimized Categorical Boosting. *Multiscale and Multidisciplinary Modeling, Experiments and Design* **2026**, *9*, 94.

ARTICLE IN PRESS

ARTICLE IN PRESS

85. Singh, M.; Choudhary, P.; Bedi, A.K.; Yadav, S.; Chhabra, R.S. Compressive Strength Estimation of Waste Marble Powder Incorporated Concrete Using Regression Modelling. *Coatings* **2023**, *13*, doi:10.3390/coatings13010066.

86. Salimbahrami, S.R.; Shakeri, R. Experimental Investigation and Comparative Machine-Learning Prediction of Compressive Strength of Recycled Aggregate Concrete. *Soft comput.* **2021**, *25*, 919–932, doi:10.1007/s00500-021-05571-1.

87. Ahmad, A.; Ahmad, W.; Chaiyasarn, K.; Ostrowski, K.A.; Aslam, F.; Zajdel, P.; Joyklad, P. Prediction of Geopolymer Concrete Compressive Strength Using Novel Machine Learning Algorithms. *Polymers (Basel).* **2021**, *13*, doi:10.3390/polym13193389.

88. Faraj, R.H.; Mohammed, A.A.; Omer, K.M.; Ahmed, H.U. Soft Computing Techniques to Predict the Compressive Strength of Green Self-Compacting Concrete Incorporating Recycled Plastic Aggregates and Industrial Waste Ashes. *Clean Technol. Environ. Policy* **2022**, *24*, 2253–2281, doi:10.1007/s10098-022-02318-w.

89. Chakravarthy HG, N.; Seenappa, K.M.; Naganna, S.R.; Pruthviraja, D. Machine Learning Models for the Prediction of the Compressive Strength of Self-Compacting Concrete Incorporating Incinerated Bio-Medical Waste Ash. *Sustainability* **2023**, *15*, 13621.

90. Sabău, M.; Remolina Duran, J. Prediction of Compressive Strength of General-Use Concrete Mixes with Recycled Concrete Aggregate. *International Journal of Pavement Research and Technology* **2022**, *15*, 73–85, doi:10.1007/s42947-021-00012-6.

91. Mohamad Ali Ridho, B.K.A.; Ngamkhanong, C.; Wu, Y.; Kaewunruen, S. Recycled Aggregates Concrete Compressive Strength Prediction Using Artificial Neural Networks (Anns). *Infrastructures (Basel).* **2021**, *6*, 1–20, doi:10.3390/infrastructures6020017.

92. Cruz, J.M.T. Dela; Rea, A.H. Dela; Magalong, C.A.S.; Poyaoan, K.A.K.; Velarde, C.M.P.; Malay, C. Coconut (Cocos Nucifera L.) Waste as Partial Coarse Aggregate Replacement for Concrete Hollow Blocks. *Asia Pacific Journal of Multidisciplinary Research* **2020**, *8*.

93. Lumbab, J.S.; Bongo, J.; Moralde, R.M.; Villaceran, G.I. Coconut Shell Ash as Partial Substitute to Cement in Concrete Hollow Blocks. In Proceedings of the IOP conference series: earth and environmental science; IOP Publishing, 2023; Vol. 1184, p. 012024.

94. Ibrahim, M. Compressive Strength Assessment of Metakaolin Hollow Sandcrete Blocks. *ARID ZONE JOURNAL OF ENGINEERING, TECHNOLOGY AND ENVIRONMENT* **2024**, *20*, 845–854.

95. Lasco, J.D.; Madlangbayan, M.; Sundo, M.B. Compressive Strength and Bulk Density of Concrete Hollow Blocks (CHB) with Polypropylene (PP) Pellets as Partial Replacement for Sand. *Civil engineering journal* **2017**, *3*, 821–830.

96. Ephraim, M.E.; Akeke, G.A.; Ukpata, J.O. Compressive Strength of Concrete with Rice Husk Ash as Partial Replacement of Ordinary Portland Cement. *Scholarly Journal of Engineering Research* **2012**, *1*, 32–36.

ARTICLE IN PRESS

97. Al-Tarbi, S.M.; Al-Amoudi, O.S.B.; Al-Osta, M.A.; Al-Awsh, W.A.; Ali, M.R.; Maslehuddin, M. Development of Eco-Friendly Hollow Concrete Blocks in the Field Using Wasted High-Density Polyethylene, Low-Density Polyethylene, and Crumb Tire Rubber. *Journal of Materials Research and Technology* **2022**, *21*, 1915–1932.

98. Olutoge, F.A. Effect of Rice Husk Ash in the Production of Hollow Sandcrete Block. *LAUTECH Journal of Engineering and Technology* **2009**, *5*, 58–63.

99. Joyklad, P.; Chatveera, B.; Ejaz, A.; Saingam, P.; Makul, N.; Hussain, Q.; Ahmadi, M.N.J.; Shrestha, K.; Sua-iam, G. Eco-Innovative Hollow Concrete Blocks with Diatomite and Sugarcane Bagasse Ash: Advancing Sustainability in Construction Material. *Engineered Science* **2025**, *35*, 1492.

100. Mitikie, B.B.; Ayalewu, W.Z.; Cherkos, F.D. Effect of Water Hyacinth Ash on Properties of Concrete Containing Superplasticizer. *Discover Civil Engineering* **2025**, *2*, 21.

101. Elsayed Ahmed Shakra, K.; Mohamed Abd Elrazike, M.; Ibrahim Mohammed Abdel Hady, M.; Mahmoud Sadek, D.; Ahmad Ibrahim Massoud, O. The Effects of Reuse Marble Waste on Hollow Concrete Blocks in Constructions. *Engineering Research Journal* **2018**, *160*, 192–205.

102. Yayena, E.; Hareru, W.K. Engineering Experimental Study on Mechanical and Durability Properties of Banana Leaves Ash as Partial Cement Replacement in Hollow Concrete Blocks. *Discover Applied Sciences* **2024**, *6*, 105.

103. Khandagale, A.S.; Aher, G.A.; Pharate, K.G. Experimental Study of Use of Water Hyacinth Ash in Concrete. *Journal of Emerging Technologies and Innovative Research (JETIR)* **2023**, *10*, 561–564.

104. Saravanan, M.M.; Sivaraja, M. Mechanical Behavior of Concrete Modified by Replacement of Cement by Rice Husk Ash. *Brazilian Archives of Biology and Technology* **2016**, *59*, e16161072.

105. Omran, A.; Soliman, N. Performance of Concrete Containing Water-Hyacinth Ash (Wha) as a Cement Replacement: Fresh and Mechanical Properties. **2025**.

106. Khamput, P.; Choosakul, C.; Klathae, T.; Rittipuakdee, S.; Monkeaw, S. Product of Hollow Concrete Blocks Mixed with Rice Husk Ash and Cassava Fermentation Waste. *ASEAN Journal of Scientific and Technological Reports* **2024**, *27*, e253838–e253838.

107. Zareei, S.A.; Ameri, F.; Dorostkar, F.; Ahmadi, M. Rice Husk Ash as a Partial Replacement of Cement in High Strength Concrete Containing Micro Silica: Evaluating Durability and Mechanical Properties. *Case studies in construction materials* **2017**, *7*, 73–81.

108. Raheem, A.A.; Sulaiman, O.K. Saw Dust Ash as Partial Replacement for Cement in the Production of Sandcrete Hollow Blocks. *Int. J. Eng. Res. Appl.* **2013**, *3*, 713–721.

109. Kamau, J.; Ahmed, A.; Ngong, K. Sulfate Resistance of Rice Husk Ash Concrete. In Proceedings of the MATEC Web of Conferences; EDP Sciences, 2018; Vol. 199, p. 02006.

ARTICLE IN PRESS

110. Sojobi, A.O.; Awolusi, T.F.; Aina, G.B.; Oke, O.L.; Oladokun, M.; Oguntayo, D.O. Ternary and Quaternary Blends as Partial Replacement of Cement to Produce Hollow Sandcrete Blocks. *Heliyon* **2021**, *7*.

111. Subba, E.R.; Kumar, E.C.; Sharma, D. Utilizing Crushed Waste Glass as A Sustainable Replacement for Fine Aggregate in Concrete.

112. Mitikie, B.B.; Alemu, Y.L.; Reda, S.G. Utilization of Basaltic Quarry Dust as a Partial Replacement of Cement for Hollow Concrete Block Production. *Int. J. Concr. Struct. Mater.* **2022**, *16*, 55.

ARTICLE IN PRESS